Neuropharmacology 205 (2022) 108898

Contents lists available at ScienceDirect

Neuropharmacology

journal homepage: www.elsevier.com/locate/neuropharm

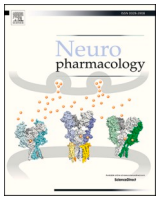

Leptin coordinates efferent sympathetic outflow to the white adipose tissue through the midbrain centrally-projecting Edinger-Westphal nucleus in male rats

Lu Xu [a,i], Nóra Füredi [b,c], Christoph Lutter [b,1,2], Bram Geenen [a], Erika Pétervári [c], Márta Balaskó [c], Ádám Dénes [d], Krisztina J. Kovács [e], Balázs Gaszner [b,*,3], Tamás Kozicz [a,f,g,h,**,3]

[a] Department of Anatomy Medical Imaging, Donders Institute for Brain, Cognition and Behaviour, Radboud University Nijmegen Medical Centre, Nijmegen, the Netherlands
[b] Department of Anatomy and Center for Neuroscience, Medical School, Pécs University, Pécs, Hungary
[c] Department of Translational Medicine, Medical School, Pécs University, Pécs, Hungary
[d] "Momentum" Laboratory of Neuroimmunology, Institute of Experimental Medicine, Budapest, Hungary
[e] Institute of Experimental Medicine, Eötvös Loránd Research Network, Budapest, Hungary
[f] Department of Clinical Genomics, Mayo Clinic, MN, USA
[g] Department of Laboratory Medicine and Pathology, Mayo Clinic, MN, USA
[h] Center for Individualized Medicine, Mayo Clinic, Rochester, MN, USA
[i] Department of Structural and Cellular Biology, School of Medicine, Tulane University, New Orleans, LA, USA

ARTICLE INFO

Keywords:
Urocortin 1
Leptin receptor
STAT3
Pseudorabies virus
Energy metabolism

ABSTRACT

The centrally-projecting Edinger-Westphal nucleus (EWcp) hosts a large population of neurons expressing urocortin 1 (Ucn1) and about half of these neurons also express the leptin receptor (LepRb). Previously, we have shown that the peripheral adiposity hormone leptin signaling energy surfeit modulates EWcp neurons' activity. Here, we hypothesized that Ucn1/LepRb neurons in the EWcp would act as a crucial neuronal node in the brain-white adipose tissue (WAT) axis modulating efferent sympathetic outflow to the WAT. We showed that leptin bound to neurons of the EWcp stimulated STAT3 phosphorylation, and increased Ucn1-production in a time-dependent manner. Besides, retrograde transneuronal tract-tracing using pseudorabies virus (PRV) identified EWcp Ucn1 neurons connected to WAT. Interestingly, reducing EWcp Ucn1 contents by ablating EWcp LepRb-positive neurons with leptin-saporin, did not affect food intake and body weight gain, but substantially (+26%) increased WAT weight accompanied by a higher plasma leptin level and changed plasma lipid profile. We also found that ablation of EWcp Ucn1/LepRb neurons resulted in lower respiratory quotient and oxygen consumption one week after surgery, but was comparable to sham values after 3 and 5 weeks of surgery. Taken together, we report that EWcp/LepRb/Ucn1 neurons not only respond to leptin signaling but also control WAT size and fat metabolism without altering food intake. These data suggest the existence of a EWcp-WAT circuitry allowing an organism to recruit fuels without being able to eat in situations such as the fight-or-flight response.

1. Introduction

Maintaining body adiposity is a physiological necessity and disturbance of tightly controlled regulation of the body's fat stores leads to obesity, a disease resulting from nutrient excess where energy intake significantly exceeds energy expenditure (Morton et al., 2006). Leptin, a

* Corresponding author. Department of Anatomy, Pécs University, Szigeti u 12., 7624, Pécs, Hungary.
** Corresponding author. Department of Clinical Genomics, Mayo Clinic, 200 1st Street, SW, Rochester, MN, USA.
E-mail addresses: balazs.b.gaszner@aok.pte.hu (B. Gaszner), Kozicz.Tamas@mayo.edu (T. Kozicz).
[1] Department of Orthopedics, Rostock University Medical Center, Rostock, Germany.
[2] School of Clinical and Applied Sciences, Leeds Beckett University, Leeds, UK.
[3] These authors contributed equally.

https://doi.org/10.1016/j.neuropharm.2021.108898
Received 12 April 2021; Received in revised form 29 September 2021; Accepted 21 November 2021
Available online 1 December 2021

hormone derived from adipocytes, conveys information about nutritional reserves to the brain, where it acts to modulate metabolism and maintain energy balance (Zhang et al., 1994; Gao and Horvath, 2007; Simerly, 2008; Myers et al., 2009). Leptin acts through the long form of the leptin receptor (LepRb), by activating various signaling pathways in distinct populations of LepRb-neurons (Niswender et al., 2004; Villanueva and Myers, 2008; Rahmouni et al., 2009). These nerve cells reside in brain areas involved in regulating energy balance, such as in the hypothalamus and brainstem (Elmquist et al., 1998; Figlewicz et al., 2006; Leinninger et al., 2009). One such area is the centrally-projecting Edinger-Westphal nucleus (EWcp) in the rostral midbrain (Scott et al., 2009; Caron et al., 2010; Xu et al., 2011). The significance of EWcp in mediating food consumption and stress-related behaviors has become increasingly acknowledged (Turek and Ryabinin, 2005; Ryabinin and Weitemier, 2006; Korosi et al., 2005; Kozicz, 2007; Kozicz et al. 2001, 2011, 2011; Rouwette et al., 2011; Xu et al. 2009, 2010, 2011, 2012, 2014; Füredi et al., 2017).

The EWcp is the major seat of urocortin 1 (Ucn1) neurons in the brain (Kozicz et al., 1998; Bittencourt et al., 1999). Ucn1 is an important modulator of metabolic functions and feeding behavior (Kuperman and Chen, 2008). Intracerebroventricular administration of Ucn1 strongly suppresses food intake (Benoit et al., 2000; Wang et al., 2001), and increases body temperature and oxygen consumption (De Fanti and Martínez, 2002). In the mouse, EWcp/Ucn1 neurons respond to *in vitro* leptin administration with a slow activation of the JAK2-STAT3 signaling pathway (Xu et al., 2011). Systemic injection of leptin increases Ucn1-content of the EWcp, whereas mice lacking LepRb exhibit decreased Ucn1 expression (Xu et al., 2011).

While most studies have been focused on leptin's action on the brain, the brain also modulates the efferent sympathetic outflow to the adipose tissue (Zhang et al., 2014). As the primary energy store, the adipose tissue plays an important role in energy balance. Histologically and functionally two distinct types of fat tissues can be distinguished: white adipose tissue (WAT) and brown adipose tissue (BAT). The WAT stores chemical energy in the form of triglycerides whereas the BAT dissipates chemical energy in the form of heat through thermogenesis (Zhang et al., 2014). Because BAT has a relatively small fat storage capacity and a high metabolic demand to support a continuous thermogenic response, it relies on continuous free fatty acids from WAT.

The sympathetic nervous system (SNS) is the main driver for adipose tissue lipolysis. In the WAT, SNS stimulation leads to the breakdown of lipids, causing smaller fat cell size and reducing leptin release. In the BAT, SNS stimulation induces lipolysis and thus Uncoupling Protein 1 (UCP1) activation (a marker for thermogenesis). Therefore, it has been hypothesized that coordinated sympathetic action of BAT and WAT would maximize leptin's effect on energy expenditure and fat metabolism (Zeng et al., 2015). However, an important research gap exists in understanding how leptin actions would be connected to the sympathetic activation of WAT and BAT.

Although the Edinger-Westphal nucleus has been traditionally considered as the parasympathetic component of the oculomotor complex (e.g. Warwick, 1954; Klooster et al., 1993), retrograde infection of EWcp neurons has been reported after pseudorabies virus (PRV) injection into the sympathetic stellate ganglion, BAT, pancreas, spleen and adrenal gland (Jansen et al., 1997; Farkas et al., 1998; Cano et al., 2001; Zhang et al., 2011; Shah et al., 2013). Besides, Ucn1 fibers occur in the lamina VII of the mouse spinal cord (Korosi et al., 2007). Importantly, the two other major Ucn1-containing brain areas, the supraoptic nucleus and lateral superior olive (Bittencourt et al., 1999) do not project to the lateral horn of the spinal cord (Tucker and Saper, 1985). These facts strongly implicate EWcp/Ucn1 neurons in controlling the sympathetic nervous system's impact on adipose tissue function (for review see: Cano et al., 2021).

Based on the above data, we hypothesized that LepRb neurons in the EWcp would form an important component of a midbrain–SNS–WAT axis. More specifically, EWcp/Ucn1 neurons would 1) receive a message via leptin about the abundance of lipids in the WAT; 2) integrate this message via second messenger systems such as JAK2-STAT3, MAPK/ERK, and PI3K/AKT to mediate EWcp neuron's activity, and modulate sympathetic tone that, in turn, would control WAT function. To test this hypothesis, we first assessed whether leptin directly bound to EWcp/Ucn1 neurons. Next, we comprehensively evaluated the effect of peripheral leptin administration on second messenger signaling (pSTAT3, pAKT, and pERK) and Ucn1 peptide and mRNA dynamics in the EWcp. To test that EWcp-Ucn1 neurons indeed innervate the WAT, we applied retrograde viral tracing. Finally, we investigated whether ablation of leptin receptor-expressing EWcp-Ucn1 neurons would influence WAT size, leptin dynamics, and metabolic parameters such as oxygen consumption, carbon dioxide production, and respiratory quotient (calorimetry).

2. Materials and methods

2.1. Animals

Studies were performed with male Wistar rats (225–390 g). Animals from our Animal Facility of the Department of Anatomy in Pécs (original breeding pairs purchased from Charles River), were used for leptin administration (28 rats), LepRb binding (8 rats), LepRb neuron ablation (32 rats) and calorimetry (8 rats). Retrograde tracing was done in 8 rats from Toxi-coop, Budapest, Hungary. Rats were housed in standard plastic cages (40 × 25 × 20 cm; 6 rats/cage) in a temperature- and humidity-controlled environment, on a 12-hrs light/12-hrs dark cycle (lights on at 6:00 AM), with free access to tap water and rat chow. They were allowed 1 week of acclimation before an experiment. The use of male rats was preferred in this study because the EWcp/Ucn1 neurons are estrogen sensitive and the effect of the estrus cycle could have influenced the results (Derks et al., 2010).

Animals were sacrificed by an overdose of anesthetic injection (sodium-pentobarbital, Nembutal, Sanofi, Budapest, Hungary; 100 mg/kg body weight). All efforts were made to minimize the number of animals used and their suffering. *In vivo* experimental procedures were permitted by the National Food Chain Safety Office in Hungary (license numbers: BA02/2000-26/2011 and BA02/2000-22/2017). The licenses were given based on the scientific approvals of the Animal Welfare Committee at Pécs University and the National Scientific Ethical Committee on Animal Experimentation in Hungary.

2.2. Cy3-labeled leptin binding

To test if leptin binds specifically to EWcp-neurons, rats were transcardially perfused with 50 ml of 0.1 M sodium phosphate-buffered saline (PBS; pH 7.4), decapitated, and their brains rapidly dissected. Then, 100 μm-thick brain sections containing the EWcp were incubated with 1 μM (n = 4 rats) or 50 nM (n = 4 rats) Cy3-labeled leptin (Phoenix Pharmaceuticals, Burlingame, CA, USA) for 20 min at 4 °C. As a negative control EWcp sections from the same rats were incubated with inactivated, Cy3-labeled leptin that was boiled for 10 min before use. Subsequently, the sections were fixed with 4% paraformaldehyde (PFA), mounted on glass slides, and analyzed with a confocal laser scanning microscope (Leica Microsystems TCS SP2 AOBS system, Wetzlar, Germany). For further details of this method, see Kieffer et al. (1997).

2.3. Leptin injection

Rats (n = 4 per group) were injected intraperitoneally (i.p.) with either leptin (3 mg/kg in sterile PBS, pH 7.4), or an equal volume vehicle, and sacrificed 0, 1, 2 or 4 h later. The dose of leptin injection was determined based on an earlier work by Rizk et al. (2001). Recombinant mouse leptin was obtained from the National Hormone and Peptide Program (Dr. A.F. Parlow, Los Angeles, CA, USA). After deep anesthetization with Nembutal (100 mg/kg body weight), they were

transcardially perfused with 50 ml of 0.1 M PBS (pH 7.4) followed by 250 ml 4% ice-cold PFA in 0.2 M Millonig sodium phosphate buffer (pH 7.4). After decapitation, brains were dissected and stored in the PFA for 2 days. Then, brains were transferred into 30% sucrose in PBS, and when completely submerged, 6 series of 25 μm-thick coronal sections were cut at the midlevel of the EWcp (5.0–7.0 mm caudal to the level of Bregma; see Paxinos and Franklin, 2003) on a freezing microtome (Microm, Walldorf, Germany), saved in sterile antifreeze solution (0.1 M PBS, 30% ethylene glycol, 20% glycerol), and stored at −20 °C until immunohistochemistry for pSTAT3, pAKT, pERK and Ucn1.

2.4. Retrograde transneuronal tract-tracing

For retrograde tracing, Ba-DupGreen (BDG), a recombinant, Bartha-derived pseudorabies virus expressing green fluorescent protein (GFP; Zs. Boldogköi, University of Szeged, Szeged, Hungary) was used (Boldogköi et al., 2002). This virus strain shows highly specific retrograde, transneuronal spread, which has been extensively characterized in our previous studies (e.g. Dénes et al., 2005; Dénes et al., 2006). Considering the spread of the virus in sympathetic circuits, upon uptake by nerve terminals in the target organ (i.e. WAT) viral capsids travel in a retrograde direction to ganglia, replicate and infect neurons that reside in the intermediolateral cell column of the spinal cord (IML). IML neurons are innervated by various autonomic nuclei in the brain stem and the hypothalamus as it has also been demonstrated in various track tracing studies using different PRV strains. BDG has special features compared to earlier PRV derivatives, as it is shows highly specific retrograde, transneuronal spread and expresses GFP with immediate-early kinetics under the regulation of the human CMV promoter, allowing early identification of infected neurons in different brain areas.

BDG virus was grown in porcine kidney (PK-15) cells to a titer of 6×10^8 plaque-forming units (PFU)/ml. BDG was concentrated to 1.5×10^{10} PFU/ml by ultracentrifugation at 70,000 g (for details see Dénes et al., 2006). The virus stocks were aliquoted and stored at −80 °C. Aliquots were thawed immediately before injection and stored at 4 °C during surgery.

Rats were anesthetized by i.p. injection of a mixture of 50 mg/kg ketamin (Richter, Budapest, Hungary), 10 mg/kg xylazin (Spofa, Praha, Czech Republic) and 5 mg/kg prometazin (EGIS, Budapest, Hungary). Epididymal WAT was exposed through an abdominal midline incision and placed onto sterile cotton wool. Then, 0.4–0.4 μl BDG was injected with a Hamilton syringe at 5 equidistant places into the WAT (sum: 2 μl). Finally, the peritoneum and abdominal wall was sutured.

Rats were housed individually and monitored twice a day. Five days later, animals were sacrificed by deep Nembutal (100 mg/kg) anesthetization and transcardially perfused with 50 ml saline followed by 400 ml ice-cold Zamboni's solution (4% PFA and 0.2% picric acid in 0.1 M PBS; pH 7.4). Brains were postfixed in the same fixative for 16 h, and cryoprotected in 10% sucrose. Four series of 30 μm thick sections were cut and were stored at −20 °C in sterile antifreeze solution as described above. Productive infection was observed in 6 rats, by identification of GFP-containing neurons along the sympathetic neuraxis (Dénes et al., 2005).

2.5. Neuron ablation

Rats were anesthetized by i.p. injection of a mixture of 78 mg/kg ketamine (Calypsol, Richter Gedeon, Budapest, Hungary) and 13 mg/kg xylazine (Sedaxylan, Eurovet Animal Health BV, Bladel, The Netherlands). Then, the scull was drilled on the left side, an incision made on the dura mater, and an injection needle stereotactically inserted at an angle of 19° from dorsolateral to ventromedial, 4.8 mm posterior and 1.5 mm lateral to Bregma. Either unconjugated saporin (53 ng in 80 nl MQ; Kit-47; Advanced Targeting Systems, San Diego, CA, USA) or leptin-conjugated saporin (90 ng in 80 nl MQ; Kit-47; Advanced Targeting Systems) was injected into the midbrain, to a depth of 5.8 mm from the dura mater, directly dorsal to the EWcp. Fourteen days later, rats were weighed, sacrificed, and their brains processed and stored in the same way as described above for the leptin injection study. Left and right epididymal WAT and BAT were collected. In case of BAT, a midline skin incision was made along the spinous processes of lower cervical and thoracic vertebrae to expose the interscapular area. Then, by careful dissection, the tissues were separated in the midline till the spinous processes of vertebrae got visible. This was conducted in order to accurately separate the left and right BAT. After dissection and removal of the right and left WAT and BAT tissues, they were weighed and cut into two pieces. One part was put in containers snap-frozen and stored at −20 °C, the other piece was immersion-fixed and embedded in paraffin. Sections of the midbrain (25 μm) were made using a vibratome as described above. Three series of 4 μm-thick sections of WAT and BAT were mounted on SuperFrost® microscope slides (Menzel-Gläser, Braunschweig, Germany) for histological stainings (see below).

2.6. Calorimetry

Rats were housed individually in metabolic chambers. Four chambers were used at the same time. O_2 consumption and CO_2 production were recorded by indirect calorimetry with an Oxymax calorimeter (Equal Flow, Columbus, OH, USA; for details of its working, see ref Füredi et al., 2017), starting with a 5-day control period before the surgery (on day 6) and ending with follow up tests in weeks 1, 3 and 5. O_2 consumption (ml/kg/min) and CO_2 production (ml/kg/min) were measured in air that had been perfused through the metabolic chamber, with 10 min intervals, except during daily chamber opening for cleaning (from 09.00 till 09.30 a.m.). O_2 and CO_2 data were averaged over 12-h periods, representing the light and the dark period, and the respiratory quotient (RQ) calculated. Bodyweight and 24-h food consumption were measured daily between 9.00 and 10.00 a.m.

2.7. Leptin titer and lipid profile

Blood samples were taken 2 weeks after surgery and the plasma tested for leptin titer and lipid profile: plasma triglycerides, cholesterol, high-density lipoproteins (HDL), low-density lipoproteins (LDL), and non-high-density lipoproteins (NHDL). Leptin was determined with a leptin ELISA kit (EZML-82K; Merck, Darmstadt, Germany). Plasma lipids were measured following standard protocols in the Department of Laboratory Medicine at our Radboudumc.

2.8. Hematoxylin-eosin staining

Standard HE staining was performed by immersing xylene-deparaffinated and alcohol-hydrated sections in hematoxylin and then in 0.1% eosin, both for 10 min. The sections were embedded in Entellan (Merck, Darmstadt, Germany).

2.9. Immunohistochemistry

Free-floating immunolabeling for Ucn1 with diamino-benzidine. In order to quantify the number of Ucn1 immunoreactive cells upon leptin-saporin treatment, 30 μm thick coronal sections were cut from in the EWcp. Upon 0.5% Triton X-100 treatment in PBS for 30 min, sections were blocked in 2% normal goat serum for 1 h and treated overnight with polyclonal rabbit anti-Ucn1 serum (1:20.000, #5779; The Salk Institute, La Jolla, CA, USA). After washes, a biotinylated goat anti-rabbit secondary antibody was used for 60 min (1:200, Vectastain Elite ABC Kit, Vector Laboratories, Inc. Burlingame, CA, USA, #PK-6101). Subsequently, peroxidase-labeled avidin-biotin complex treatment was carried out (Vectastain Elite ABC Kit, #PK-6101) for 60 min. The immunolabeling was developed in Tris buffer containing 0.03% (v/v) H_2O_2 and 0.02% (m/v) 3, 3′diamino-benzidine (DAB) for 7 min. After

PBS washes, sections were mounted on gelatin-coated slides, air dried, dehydrated in 30%, 50%, 70%, 96% and absolute alcohol solutions (5 min, respectively), cleared in xylene for 2 × 10 min and cover-slipped with Depex.

Immunofluorescence. Phosphorylated anti-Hormone-Sensitive Lipase (p-HSL) staining. After deparaffinization, sections were incubated in Tris-buffered saline (TBS) with 0.1% Triton X-100 (TBS-T), for 1 h, blocked in 2% normal donkey serum (NDS) in TBS-T (TBS-TD), for 1 h, and incubated in primary rabbit anti-pHSL (Ser 563; 1:100), for 16 h. This was followed by 2 h incubation with secondary donkey anti-rabbit-Alexa Fluor 647 serum (1:200). Next, sections were incubated in DAPI (1 μg/ml), for 10 min, and embedded in Entellan.

For single immunolabeling of Ucn1, pAKT or pERK, free-floating sections were treated with 0.5% Triton X-100 in PBS, for 30 min, blocked in 2% NDS, for 1 h, and incubated in primary antiserum goat anti-Ucn1 (1:100) or rabbit anti-pAKT (1:100) or rabbit anti-pERK (1:300) respectively, for 16 h. This was followed by 2 h incubation with secondary Cy2-conjugated anti-goat IgG (1:100) or Cy3-conjugated anti-rabbit serum (1:100). For single immunolabeling of pSTAT3, sections were pretreated sequentially with 3% H_2O_2/1% NaOH, for 20 min, 0.3% glycine, for 10 min, and 0.03% SDS, for 10 min, and processed as described above with primary rabbit anti-pSTAT3 (1:500) and Cy3-conjugated anti-rabbit IgG secondary sera (1:100).

To reveal WAT innervating Ucn1 neurons, double immunolabeling of GFP and Ucn1 was performed. EWcp sections were processed as described for single immunolabeling, but with incubation in a mixture of primary chicken anti-GFP serum (1:2000) and primary rabbit anti-Ucn1 serum (1:30,000), for 16 h, and then in a mixture of Cy2-conjugated anti-chicken and Cy3-conjugated anti-rabbit sera (1:100) for 2 h. Finally, sections were mounted on gelatin-covered slides, air dried and coverslipped with a few drops of FluorSave™ (Merck).

2.10. Antisera and immunohistochemistry controls

Polyclonal rabbit anti-Ucn1 serum was a generous gift from Dr. W.W. Vale† (#5779; The Salk Institute, La Jolla, CA, USA, RRID AB_2313740). Monoclonal chicken anti-GFP was from Abcam (#13970; Cambridge, MA, USA, RRID AB_300798), polyclonal rabbit anti-pAKT Ser473 (#4058, RRID AB_331168), rabbit anti-pSTAT3 Tyr705 (#9131, RRID AB_331586) and rabbit anti-pHSL (Ser563; #4139 RRID AB_2135495) from Cell Signaling Technology (Danvers, MA, USA), and polyclonal rabbit anti-pERK Tyr204 (#7976, RRID AB_2297323) and goat anti-Ucn1 (#sc-1825, RRID AB_2304014) from Santa Cruz Biotechnology (Santa Cruz, CA, USA). NDS, Cy2-conjugated donkey-anti-mouse (#715-225-151, RRID AB_2340827), Cy2-conjugated donkey-anti-goat (#705-225-147 RRID AB_2307341), Cy2-conjugated donkey-anti-chicken (#703-225-155, RRID AB_2340370), and Cy3-conjugated donkey-anti-rabbit (#711-165-152, RRID AB_2307443) sera were obtained from Jackson ImmunoResearch (West Grove, PA, USA) and Alexa Fluor 647-conjugated donkey-anti-rabbit serum (#A31573, RRID AB_2536183) from Thermo Fisher Scientific.

The specificity of the Ucn1 antisera (#5779 and #sc-1825) was tested earlier in the rat (Gaszner et al., 2004; Füredi et al., 2017). pAKT (#4058, Xu et al., 2011), pSTAT3 (#9131, Xu et al., 2011) pHSL (#4139, Xu et al., 2011), and pERK (#7976, Xu et al., 2011) sera are also well-trusted widely used antibodies for immonolabelings. Omission and replacement of primary and secondary antibodies with respective non-immune sera abolished the signal in all pre-tests in this experiment also.

2.11. In situ hybridization

In situ hybridization of Ucn1 mRNA was carried out on free-floating sections, as follows. Antisense and sense (control) RNA probes were generated using a linearized 550 bp Ucn1 cDNA, subcloned in pBluescript (Stratagene, Agilent Technologies, Santa Clara, CA, USA), and labeled with DIG-11-UTP using a labeling kit from Roche Molecular Biochemicals (Basel, Switzerland). Sections were fixed in 0.1 M borax-buffered 4% PFA (pH 9.5), at 4 °C for 30 min, and rinsed 4 × 7 min in 0.1 M PBS. After rinsing in autoclaved MQ water, acetylation was performed with 0.25% acetic acid anhydride in 0.1 M tri-ethanolamine buffer (pH 8.0), for 10 min, followed by rinsing in 2 times (2 ×) concentrated standard saline citrate buffer (SSC; pH 7.0), for 5 min. Hybridization mixture (50% deionized formamide, 0.3 M NaCl, 0.001 M EDTA, Denhardt's solution, 10% dextran sulphate; pH 7.0) together with 0.5 mg/ml tRNA and the mRNA-digoxigenin (DIG) probe (2.5 ng/ml), were placed in a water bath at 80 °C for 5 min, and then on ice for another 5 min. Sections were incubated in hybridization solution, for 16 h at 60 °C, rinsed 4 × 7 min with 4 × SSC, incubated for 30 min at 37 °C in preheated RNAse A medium (0.5 M NaCl, 0.01 M Tris/HCl, 0.001 M EDTA, 0.01 mg/ml RNAse A; pH 8.0) that had been added just before the start of incubation, and stringently rinsed in steps with decreasing SSC concentrations (2 × , 1 × , 0.5 × , 0.1 ×), for 30 min at 58 °C. DIG-label was detected with the alkaline phosphatase method with nitroblue tetrazolium chloride/5-bromo-4-chloro-3-indolyl phosphate-toluidine salt (NBT/BCIP) as substrate. Briefly, after rinsing 4 × 5 min with buffer A (0.1 M Tris/HCl, 0.15 M NaCl; pH 7.5) sections were pre-incubated in buffer A containing 0.5% blocking agent (Roche) for 1 h, followed by 3 h incubation with sheep anti-DIG-AP (Roche; 1: 5000) in buffer A containing 0.5% blocking agent. Subsequently, sections were rinsed 4 times in buffer A, for 5 min, followed by 2 times 5 min rinsing in buffer B (0.1 M Tris/HCl, 0.15 M NaCl, 0.05 M $MgCl_2$; pH 9.5). After 6 h incubation in NBT/BCIP medium (10 ml buffer B, 2.4 mg levamisole, 175 ml NBT/BCIP mixture; Roche) in a light-tight box, the reaction was stopped by placing the sections in buffer C (0.1 M Tris/HCl, 0.01 M EDTA; pH 8.0). Sections were mounted on gelatin coated slides and embedded using Kaiser's glycerol gelatin (Boom Chemicals).

2.12. RNA extraction from adipose tissue and cDNA synthesis

Small pieces of WAT or BAT (~1–10 mm^3) were used for RNAse-free RNA isolation. Tissue was incubated with 500 μl TRIzol® (Invitrogen) on ice, for 30 min, crushed using small glass cylinders, and sonificated to maximize RNA yield in an Ultrasonic processor (Sonics & Materials, Newton, USA), for 30 s. After adding 200 μl chloroform, the sample was centrifuged for 15 min at 4 °C, at 14,000 rpm. The aqueous phase was incubated for 10 min at 20 °C with 1 μl (20 μg) of glycogen (Thermo Fisher Scientific, Waltham, MA, USA) and 500 μl iso-propanol, and centrifuged again at 4 °C and 14,000 rpm, for 10 min. The cell pellet was rinsed for 1 min with 1 ml 75% ethanol, centrifuged at 4 °C and 14,000 rpm, for 5 min, air-dried, dissolved in 50 μl diethyl pyrocarbonate (DEPC)-treated MQ water, and its RNA concentration determined with a ND-1000 spectrophotometer (NanoDrop, Wilmington, USA).

For cDNA synthesis 100 ng isolated RNA was incubated in 11 μl DEPC-treated MQ with 1 μl (0.25 mU) random primers (Roche), for 10 min at 70 °C. Then, a mixture of 4 μl First Strand Buffer (5x), 2 μl of 10 mM dithiothreitol, 0.5 μl Rnasin (RNAse inhibitor), 0.5 μl (100 U) Superscript II (all from Invitrogen) and 1 μl (0.5 mM) dNTPs (Roche) was added. cDNA synthesis was done for 75 min at 37 °C and ended by putting the samples at 95 °C, for 10 min. cDNA was stored at −20 °C.

2.13. Quantitative RT-PCR

Q-PCR was performed with a 7500 Real-Time PCR machine (Applied Biosystems, Foster City, USA), in FrameStar 96 well plates (4titude, Surrey, UK) filled with a mixture of 1.5 μl DEPC-treated MQ, 12.5 μl Power SYBR® Green mixture (2x; Applied Biosystems) and 3 μl (15 pmol) UCP1 (forward CAGAACTCACCGCTCAACAG, reverse ATCCATGGACGTTGCTTGTC) or ADRB3 (forward CCACAGAAAGCTTGTCAACACT, reverse AATGGCAGGGGACGTCAT) primers (both from Biolegio, Nijmegen, The Netherlands) to which 5 μl cDNA had been added. As a reference gene, ribosomal subunit 18S was used

(forward: TTGCTGATCCACATCTGCTGG, reverse ATTGCCGACAGGATGCAGAA) as this housekeeping gene appeared to be reliable (Derks et al., 2008). The reaction cycle was as follows: a single denaturation step of 10 min at 95 °C, followed by 40 repetitions of 15 s of denaturation at 95 °C and 1 min of elongation at 60 °C. Next, dissociation was performed during 15 s at 95 °C, 1 min at 60 °C, and finally 15 s at 95 °C. qPCR data were analyzed using the Applied Biosystems 7500 PCR machine SDS 10 software. The $2^{-\Delta\Delta Ct}$ method has been applied to further evaluate the gene expression after assessment of melting curves.

2.14. Image analysis

Images were made with either an Orthoplan light microscope (Leitz, Wetzlar, Germany) equipped with a DFC420C digital camera (Leica Microsystems, Wetzlar, Germany), or a DM IRE2 inverted fluorescence microscope (Leica). For quantitation of the amount of immunoreactive material in the EWcp, two parameters were studied: 1) the total number of immunoreactive neuronal profiles present in 4 coronal sections of the EWcp between −5.5 mm and −6.5 mm to the Bregma, and 2) per neuron, the specific immunoreactivity (ir) signal density (SSD) averaged over all neurons present in these sections, using Image J software (version 1.37, NIH, Bethesda, MD, USA). The SSD was corrected for background density outside the EWcp and expressed in arbitrary units per neuron. Measuring the size of adipocytes was done using the ImageJ software. Sizes of adipocyte fat vacuoles were expressed as the average of measurements performed by two independent observers.

2.15. Statistics

Data are presented as means with the standard error of the mean (SEM). Data shown in Figs. 3–5 were analyzed by two-way analysis of variance (ANOVA), with 'leptin' and 'time' as independent variables, preceded by tests for normality (Shapiro-Wilk test; Shapiro and Wilk, 1965) and homogeneity of variance (Bartlett's Chi-square test; Snedecor and Cochran, 1989), followed by Fisher's *post hoc* analysis (Stat Soft, Tulsa, OK, USA) ($\alpha = 5\%$). Datasets in Figs. 7–10 were evaluated using two-tailed type 2 Student's t-test after testing for normality and variance.

3. Results

3.1. The sensor: leptin binds to EWcp neurons

Previously we showed that approximately ~45% of EWcp-Ucn1 neurons expressed the short form of leptin receptor and responded to i.p. leptin injection (Xu et al., 2011). However, to study that leptin can physically bind to leptin receptor on EWcp-Ucn1 neurons and its effect on Ucn1 neuronal structure and function is not mediated by indirect neuronal pathways, we incubated acute midbrain slices containing the EWcp with Cy3-labeled leptin. Cy3-labeled leptin binding was present in the EWcp. Cy3-labeled leptin in 1 μM concentration caused a clear strong labeling of EWcp neurons. The 50 nM Cy3-labeled leptin provided a punctate cell surface signal in the EWcp (Fig. 1). This provides evidence that leptin binds to leptin receptor on EWcp-Ucn1 neurons.

3.2. The integrator: effect of leptin administration on EWcp-Ucn1 neuronal signaling

Previously, we reported that leptin activated STAT3 signaling in the EWcp-Ucn1 neurons within 2–4 h of i.p. injection (Xu et al., 2011). However, previous research has shown that leptin also recruits intracellular pathways other than STAT3 (for review see Liu et al., 2018). To obtain a comprehensive understanding of intracellular signaling pathway(s) recruited by leptin, we assessed the presence and dynamics of pSTAT3, pAKT and pERK, in a time-dependent manner. Leptin crosses the blood-brain barrier with differential dynamics (Banks et al., 2000; Faouzi et al., 2007). Therefore, we examined brain samples 0, 1, 2 and 4 h after leptin injection. To validate our approach, we first investigated the widely characterized and validated effect of i.p. leptin on pSTAT3 activation in the mediobasal hypothalamus (MBH), with saline-injected rats as controls. In line with previous literature (Xu et al., 2011), the strongest pSTAT3-ir in neuronal cell nuclei was observed 2 h after

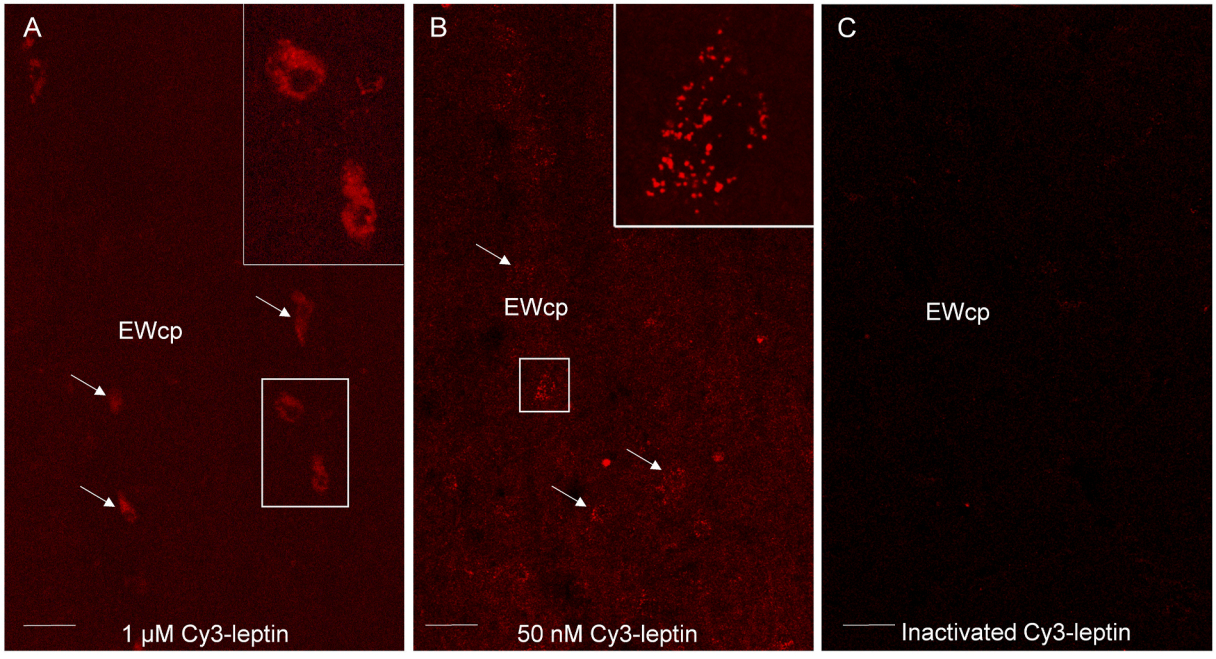

Fig. 1. Leptin binds to neurons in the centrally-projecting Edinger-Westphal nucleus (EWcp). Representative confocal images of acute slices of the rat brain treated with 1 μM (A) and 50 nM (B) Cy3-conjugated leptin. Note that the red immunofluorescence marks neuronal perikarya in the EWcp area suggesting that leptin binds to its receptors (see also higher magnification inserts). As a control, inactivated (boiled) Cy3-conjugated leptin treatment was performed that did not give any detectable red signal (C). Bars 30 μm.

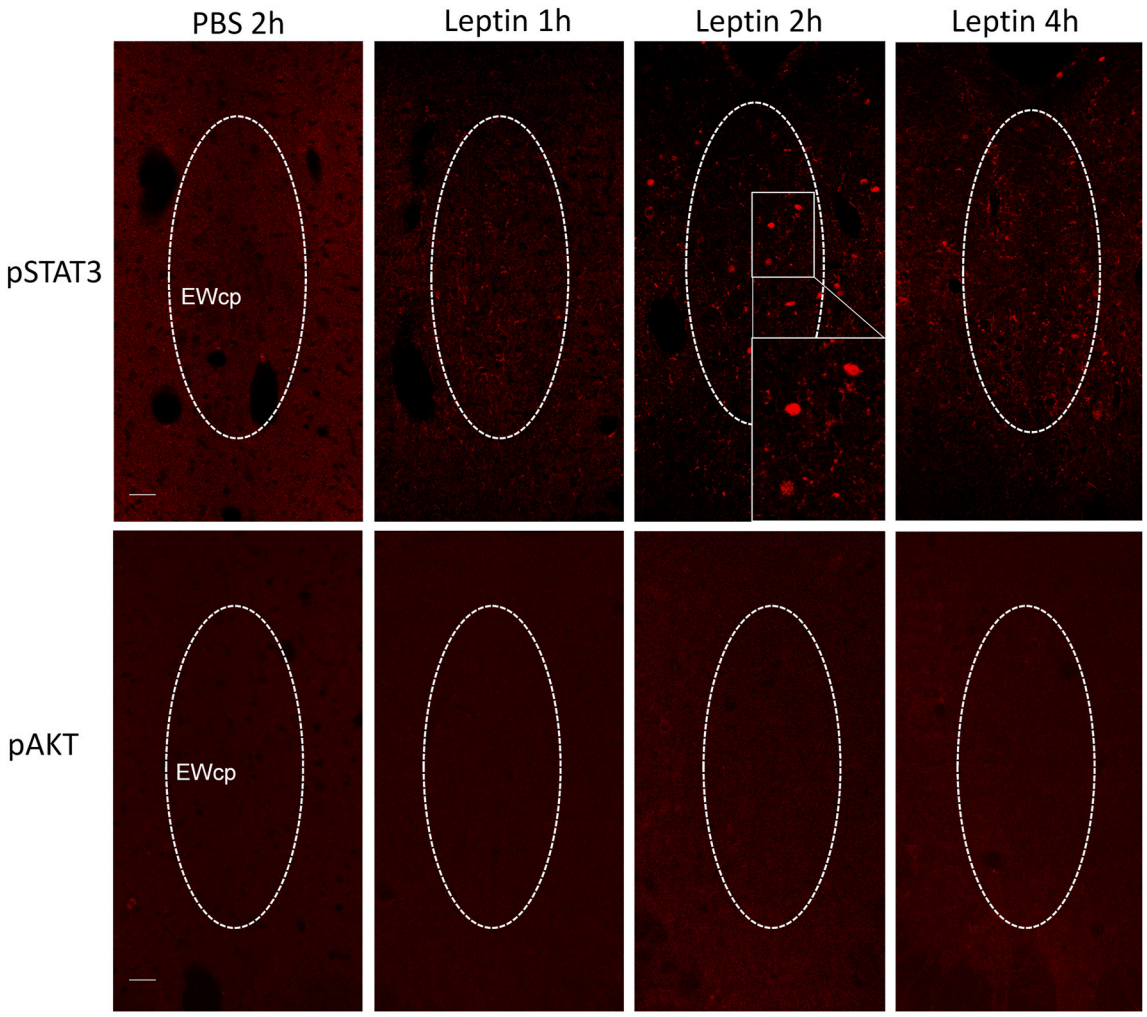

Fig. 2. Dynamics of pSTAT3 and pAKT immunoreactivity in the centrally-projecting Edinger-Westphal nucleus (EWcp) upon leptin injection. Two hours after leptin injection pSTAT3 immunoreactivity (red neuronal nuclei) appeared in the EWcp. No remarkable pSTAT3 immunosignal was detected in phosphate buffered saline-treated (control) rats and in leptin-injected animals at any other time points. Leptin injection did not induce pAKT protein expression in the EWcp at any groups and time points. Bars: 30 μm.

injection (Supplementary Fig. 1). Similarly, the most robust activation of pSTAT3 in the EWcp was observed at 2 h (Fig. 2), whereas no immunopositive cell nuclei were seen at 1 h and 4 h (Fig. 2). Saline-injected rats did not show pSTAT3-ir either in MBH or EWcp at any time points.

In line with literature data, in the MBH, leptin administration induced pAKT-ir relative to saline-treated animals, with a maximal effect at 4 h (Supplementary Fig. 1). Interestingly, no pAKT-ir was observed in the EWcp at any time point after leptin administration (Fig. 2) suggesting that leptin does not recruit the AKT signaling pathway in the EWcp.

As to the number of pERK-ir neurons, ANOVA revealed main effects of 'leptin' ($F_{1,23} = 9.45$; $P < 0.01$) and 'time' ($F_{3,23} = 5.14$; $P < 0.01$), and a leptin × time interaction ($F_{3,23} = 3.25$; $P < 0.05$; Fig. 3I). For the saline group (Fig. 3A–D), we observed no difference at any time point, but in the leptin group (Fig. 3E–H) after 4 h the number of pERK-positive neurons was markedly lower than at 0 h (−71%; $P < 0.05$), 1 h (−79%; $P < 0.0005$) and 2 h (−74%; $P < 0.01$), and markedly lower (−78%; $P < 0.01$) than in the saline group (Fig. 3I). As to the SSD of the pERK-ir neurons, ANOVA revealed an effect of time ($F_{3,23} = 7.26$; $P < 0.005$; Fig. 3J) because 1 h after leptin injection, pERK-ir was higher in both the saline (+40%; $P = 0.06$) and leptin (+53%; $P < 0.05$) group than at time point 0. This effect was only transient, as at later time points pERK-ir was not significantly different from that of the controls. While at 4 h pERK-ir in saline-injected animals was comparable to that at time point 0, in leptin-injected rats, the pERK-ir was markedly lower (−59%; $P < 0.005$).

These results provide additional evidence that leptin directly recruits EWcp-Ucn1 neurons and primarily recruits STAT3 and pERK signaling pathways.

3.3. *The integrator: effect of leptin administration on Ucn1 mRNA and peptide abundance*

Previously we reported that leptin increased Ucn1 protein expression 4 h after i.p. leptin injection (Xu et al., 2011). To show that such a leptin-mediated increase in Ucn1 peptide abundance is accompanied by increased mRNA expression, we quantitatively assessed the Ucn1 mRNA content of the EWcp neurons using *in situ* hybridization. We found a clear hybridization signal in EWcp neurons (Fig. 4). The strength of hybridization was quantified by counting the number of mRNA-expressing neurons and determining the neuronal SSD of the hybridization signal. We found no effects of leptin or time or a leptin × time interaction on the number of neurons (Fig. 4I). However, the SSD of the neurons showed effects of leptin ($F_{1,24} = 11.46$; $P < 0.005$) and time ($F_{3,24} = 3.71$; $P < 0.05$) as well as a leptin × time interaction ($F_{3,24} = 3.5$; $P < 0.05$; Fig. 4E–H). In saline-injected rats, the SSD revealed a tendency to increase at 1 h after injection (+18%; $P = 0.09$; Fig. 4J), but at 4 h it was significantly lower than at 1 h (−32%; $P < 0.005$) and 2 h (−22%; $P < 0.05$). In the leptin group, at 1 h, the SSD was higher than at

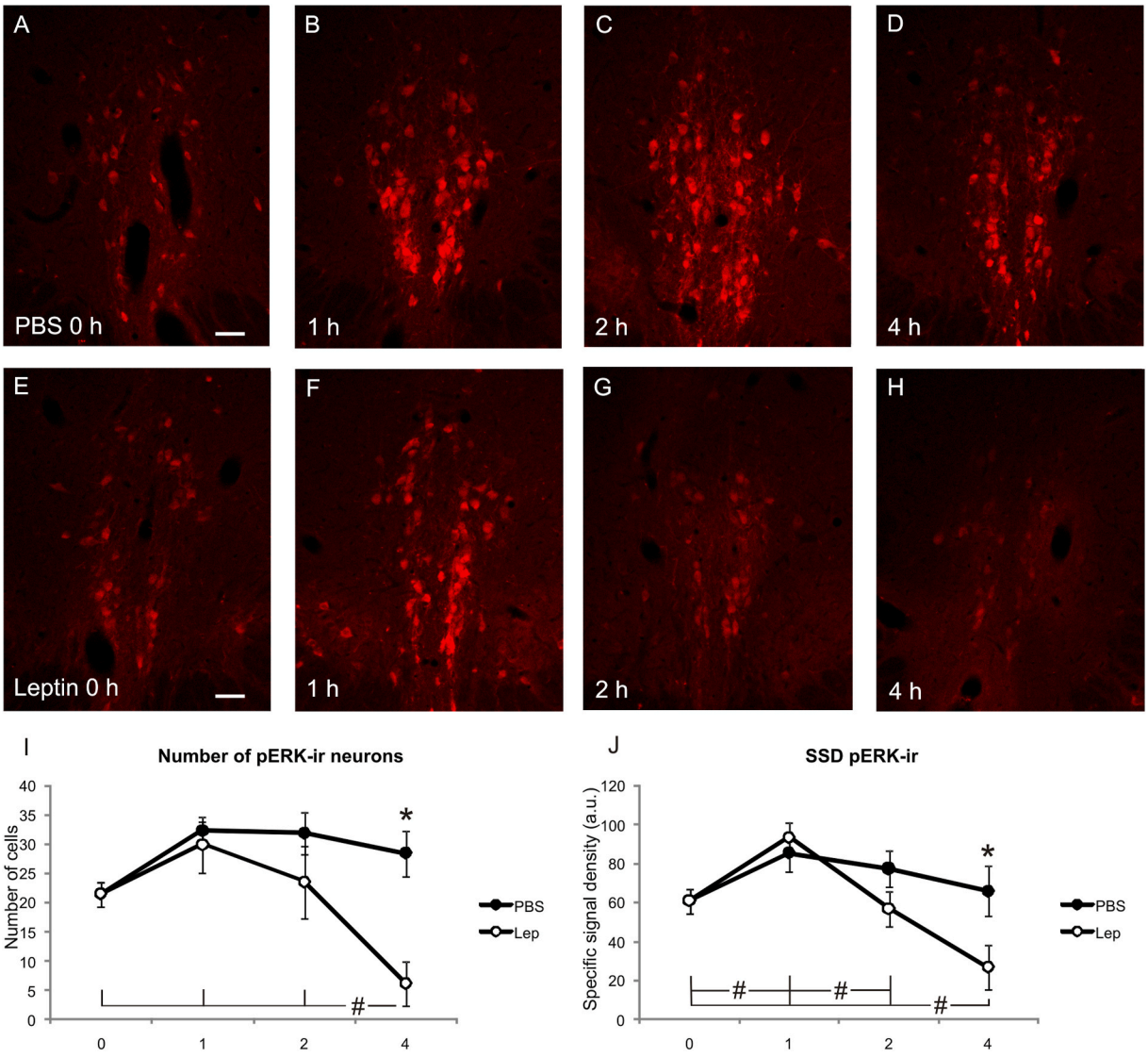

Fig. 3. Dynamics of pERK immunoreactivity in the centrally-projecting Edinger-Westphal nucleus (EWcp) in saline (PBS) vs. leptin treated rats. PBS injection (A–D) did not affect the count of pERK immunoreactive cells (closed circles in panel I). After a transient strong tendency of increase at 1 h, the specific signal density (SSD) of pERK remained stable at any time points (closed circles in J) in PBS-injected animals. In contrast, 4 h after leptin injection (F) the number of pERK-immunoreactive cells decreased compared to all time points (closed circles in graph I; #$P < 0.05$). The pERK-SSD transiently increased 1 h after leptin injection (F) followed by a strong decrease at 4 hs (see closed circles in graph J; #$P < 0.05$ compared to all other time points). Leptin-treated rats showed significantly lower pERK cell count and SSD than PBS injected animals at 4 h (*$P < 0.01$). Bars: 50 μm.

time 0 (+24%; $P < 0.05$) and stayed at that level at 2 and 4 h. As a result of these time-dependent responses in both groups, 4 h after injection the SSD was markedly higher (+54%) in the leptin group than in the saline group ($P < 0.0005$).

To determine the amount of Ucn1 peptide in the EWcp in response to leptin injection, we measured the numbers and SSD of the respective Ucn1-ir neurons. For the number, no effect of leptin and time or a leptin × time interaction was observed at any time point after injection (Fig. 5). However, the SSD revealed an almost significant effect of leptin ($F1,24 = 3.74$, $P = 0.06$) and *post hoc* analysis showed that after 4 h ($P < 0.05$), the SSD of Ucn1-ir neurons was markedly higher (+48%) in the leptin-injected rats than in the controls (Fig. 5).

These results confirm our previous observation, and reveal that leptin first increased Ucn1 mRNA expression followed by increased Ucn1 peptide abundance.

3.4. The effector - retrograde tracing from WAT

Pre-sympathetic outflow from EWcp has been previously established towards the stellate ganglion, BAT, pancreas, and spleen (Jansen et al., 1997; Farkas et al., 1998; Cano et al., 2001; Zhang et al., 2011). To explore whether EWcp/Ucn1 neurons are a source of pre-sympathetic innervation to the WAT too, we injected PRV coupled with BDG into the epididymal fat pad. Five days later, we found strong GFP-ir in EWcp, indicating productive infection and the presence of BDG. Each mid-level section of the EWcp showed about 10 immunopositive neurons (Fig. 6A, D). Double immunolabeling demonstrated that about 80% of the labeled neurons were Ucn1-positive (Fig. 6C, F).

These results strongly suggest that EWcp-Ucn1 neurons provide a higher-order pre-sympathetic innervation of WAT.

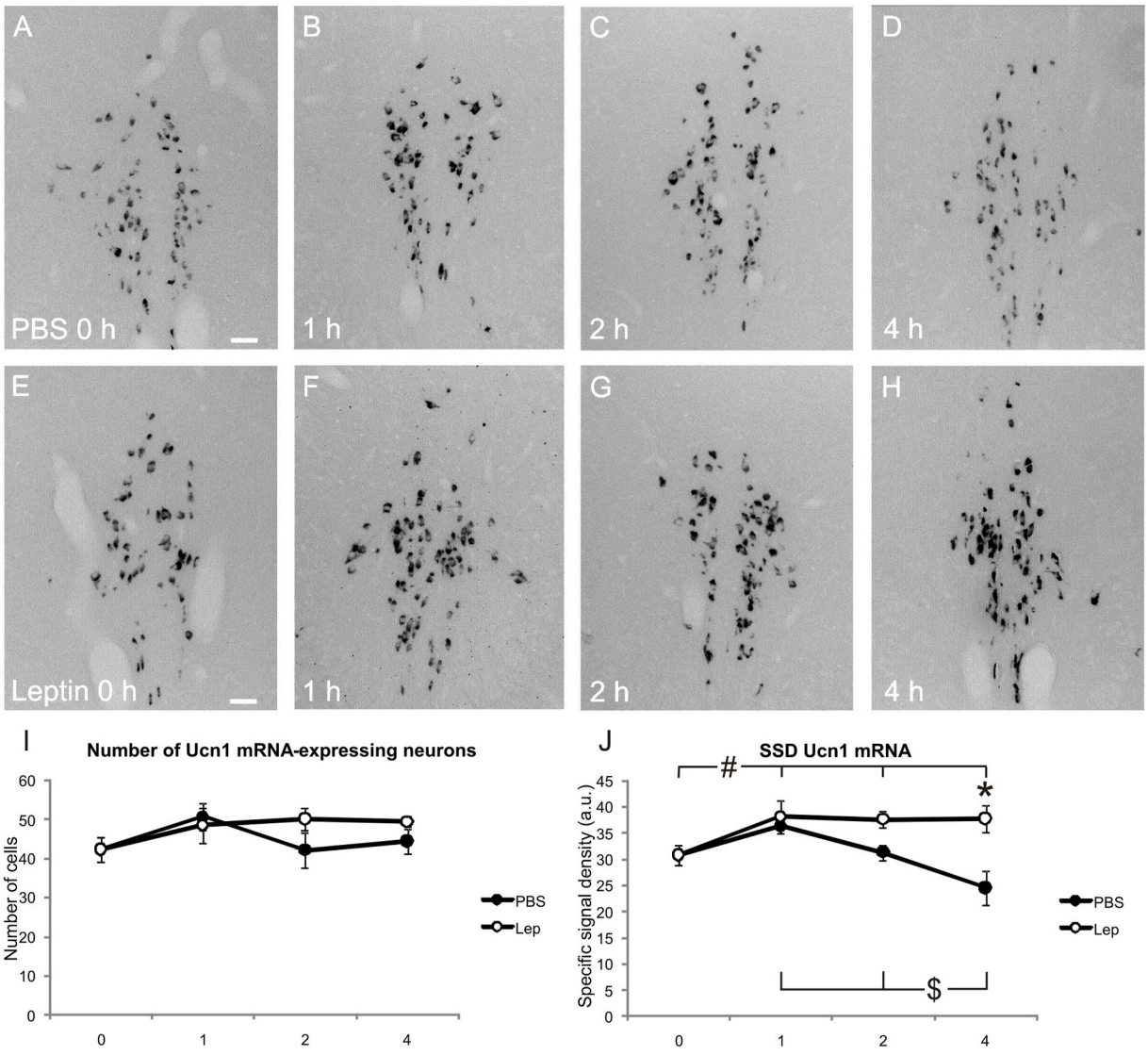

Fig. 4. *In situ* hybridization for *Ucn1* mRNA expression in the EWcp upon saline (PBS) and leptin injection at different time points. The number (I) of Ucn1 mRNA-expressing cells was not affected by PBS or leptin treatment. One hour after PBS injection (B), a trend of *Ucn1* mRNA expression increase was observed, that decreased at later time points (C, D and closed circles in graph J; $P < 0.05). Leptin injection (E–H) increased the *Ucn1* mRNA content of the EWcp at 1 h (F) that remained stable at the later time points (G, H and open circles in J; #P < 0.05). Leptin-treated rats showed significantly lower Ucn1 mRNA SSD than PBS-injected animals at 4 h (*P < 0.0005). a.u: arbitrary unit. Bars: 50 μm.

3.5. The effector – the impact of EWcp/LepRb/Ucn1 neurons on white adipose tissue

To assess EWcp/LepRb/Ucn1 neurons' functional effects on WAT, we injected leptin-conjugated saporin toxin into the EWcp. Successful ablation of LepRb-positive EWcp neurons was assessed by Ucn1-immunohistochemistry. As it is rather difficult to perform a midline injection into the EWcp without damaging the superior sagittal sinus, we recently developed an oblique approach (for details see ref. Füredi et al., 2017). With this, our success rate was about 60% with rats revealing a good injection site targeting the EWcp.

Leptin-saporin injected rats exhibited ~34% less EWcp/LepRb/Ucn1-ir neurons than controls (saporin-injected) ($t(11) = 3.397$, $P < 0.005$; control: 25.15 ± 0.83; ablation: 16.63 ± 2.2; Fig. 7A). As previously reported, approximately 45% of the Ucn1 neurons are LepRb positive (Xu et al., 2011), which means that the leptin-conjugated saporin injection had successfully ablated the majority (34/45; 75%) of the LepRb positive EWcp/Ucn1 neurons (Fig. 7A').

EWcp/Ucn1 neuronal ablation resulted in increased weight of the right WAT (+26%; $t(11) = -2.162$; $P < 0.05$; control: 0.125 ± 0.012; ablation: 0.158 ± 0.01; the weights of left and right of WAT were corrected for body weight) compared to controls (Fig. 7B). We found no significant effect in the left WAT.

Next, we tested whether LepRb/Ucn1 neuron ablation influences WAT size. We counted the number of WAT cells in HE-stained WAT sections. WAT adipocytes showed a relatively large variation in their size both in control and in leptin-saporin-treated rats. In rats with EWcp/LepRb/Ucn1 neuron ablation, we observed a larger number of large adipocytes and fewer small adipocytes than controls on both left and right WAT ($P < 0.05$). This change in WAT size-frequency distribution was also mirrored by the mean adipocyte surface area, which showed 25% increase for the left WAT and a 20% increase for the right WAT, compared to the controls ($P < 0.05$; Fig. 7D and E).

Finally, we also assessed lipolysis in WAT by measuring p-HSL-ir in the right WAT. HSL is the main player involved in the lipolytic pathways. No effect of leptin-saporin injection on the density of p-HSL-ir was observed ($P = 0.42$; control: 35.33 ± 4.03; ablation: 37.29 ± 5.61; Fig. 7C) suggesting that the ablation of EWcp-Ucn1 neurons does not

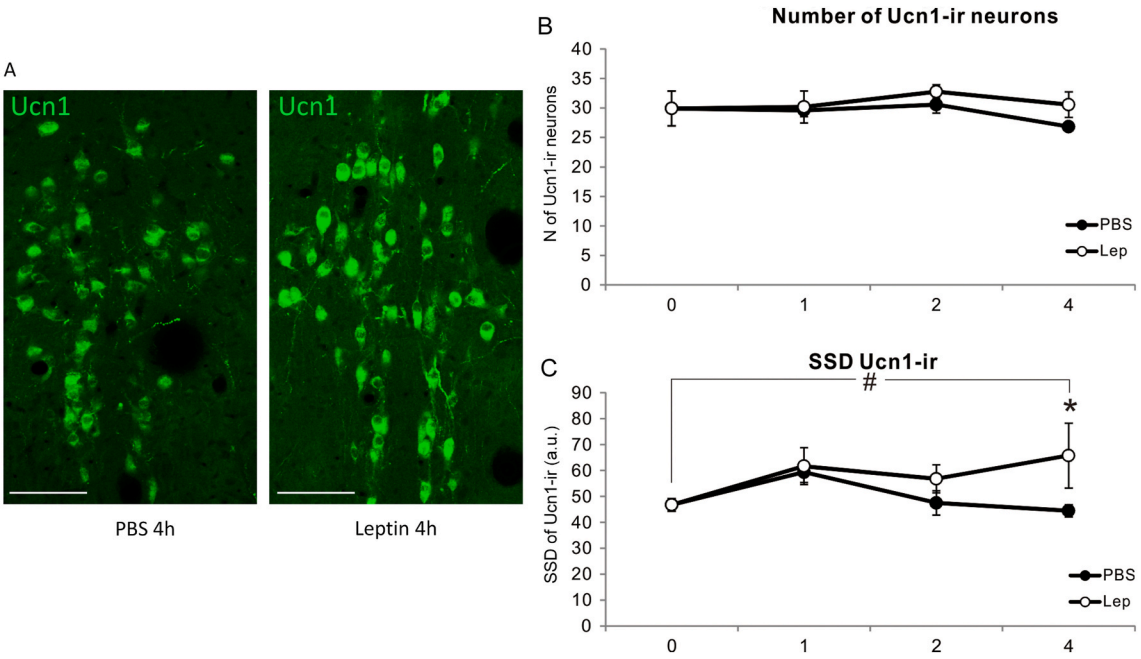

Fig. 5. Semi-quantitative immunofluorescence for Ucn1 peptide in the centrally-projecting Edinger-Westphal nucleus (EWcp) upon saline (PBS) and leptin (lep) treatment. Representative images of Ucn1 neurons (green) (A) in the EWcp 4 h upon PBS and leptin injection. The Ucn1-immunoreactive (ir) cell count was not affected by the treatment at any time points (B). The Ucn1 peptide content of the cells was significantly higher at 4 h (*$P < 0.05$), compared to the PBS-injected rats. SSD: specific signal density; a.u: arbitrary unit. Bars: 100 μm.

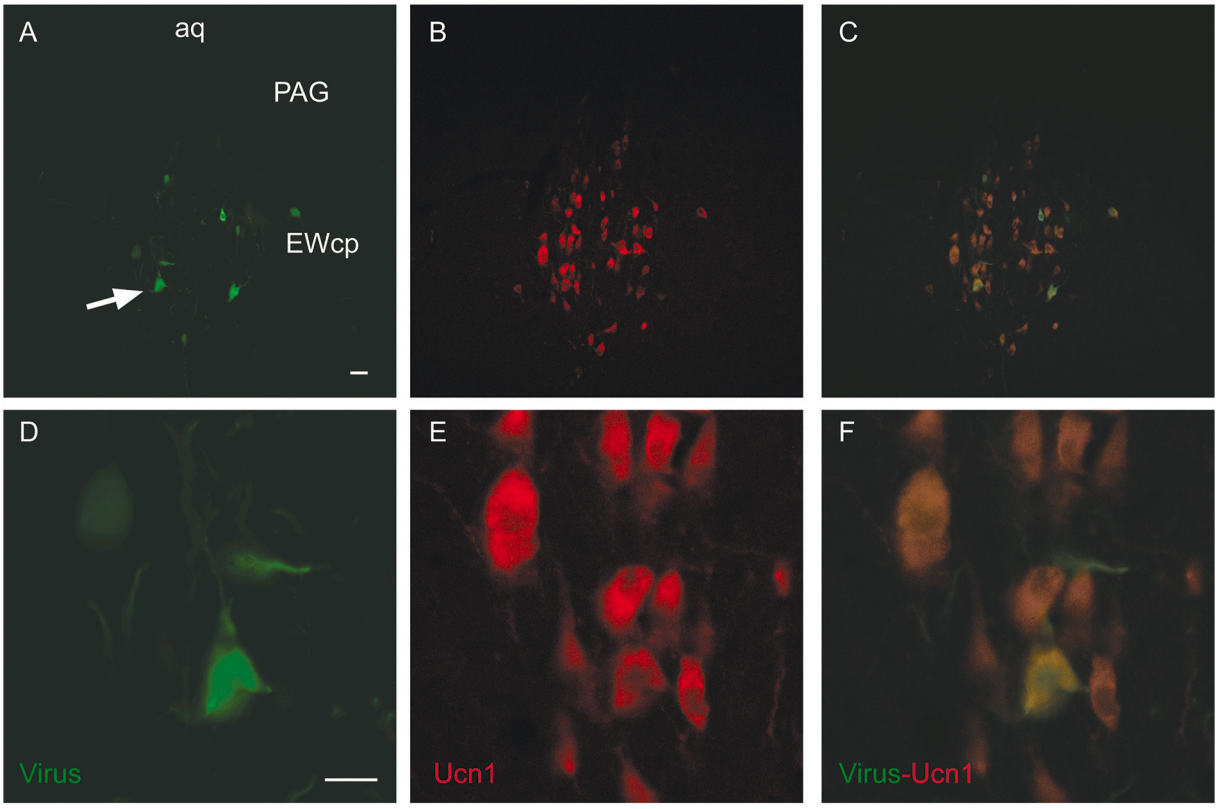

Fig. 6. Ucn1 neurons innervate the white adipose tissue. Green fluorescent protein (GFP) (A, D) appeared in the neurons of the centrally-projecting Edinger-Westphal nucleus (EWcp) after injection of GFP-expressing pseudorabies virus (Virus) into the white adipose tissue. The immunolabeling for Ucn1 peptide (B, E; red) revealed that most of the virus-infected cells were immunopositive for Ucn1 also (C, F). Bars: 30 μm.

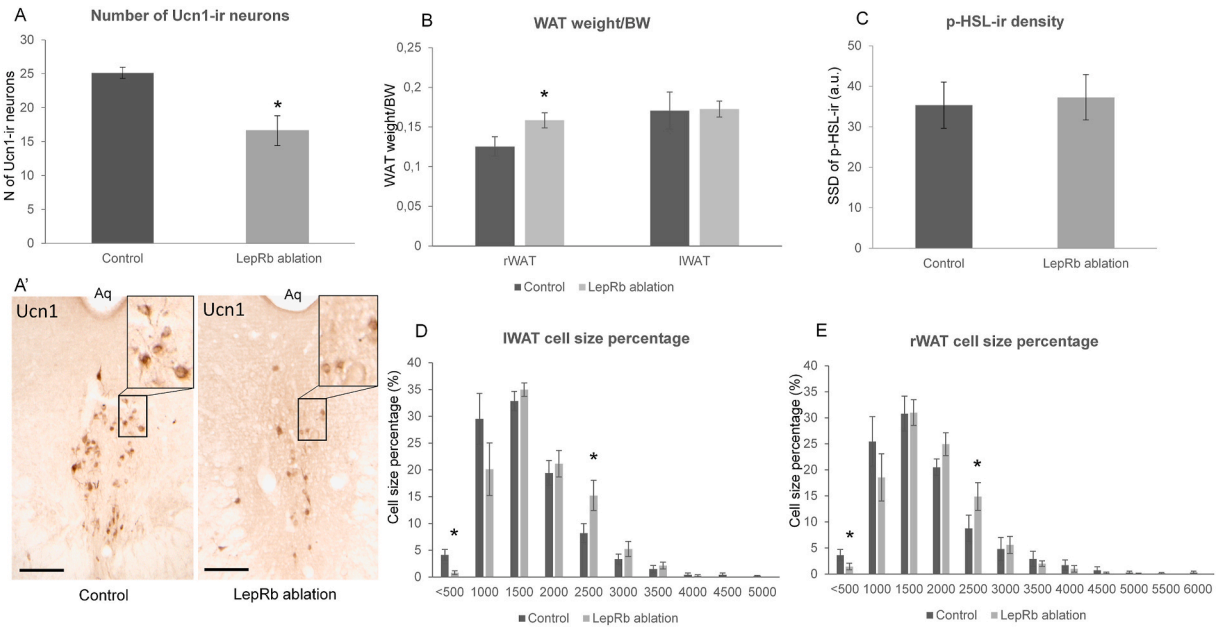

Fig. 7. Effects of EWcp/LepRb/Ucn1 neuron ablation on the white adipose tissue. Leptin-conjugated saporin treatment (A) causes a significant (*P < 0.005) reduction of Ucn1 cell counts in the centrally-projecting Edinger-Westphal nucleus (EWcp) as also shown by representative histological images in panel A'. Panel B shows bodyweight (BW)-corrected relative weight of the white adipose tissue (WAT). The right (rWAT) weight increased (*P < 0.05) upon leptin-saporin treatment of the EWcp, unlike and left (lWAT). Panel C: pHSL immunoreactivity in the WAT. Comparison of white fat cell size in the lWAT (D) and rWAT (E). Aq: cerebral aqueduct. Bars: 100 μm.

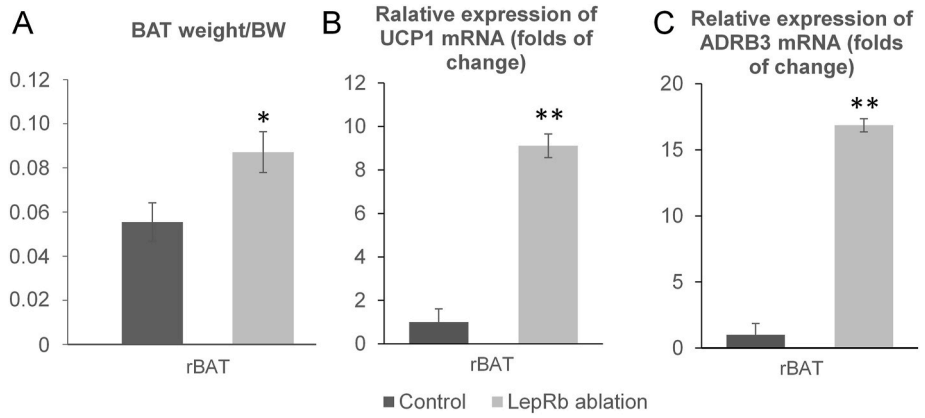

Fig. 8. Effects of EWcp/LepRb/Ucn1 neuron ablation on the brown adipose tissue (BAT). A: The bodyweight (BW)-corrected relative weight of the right (rBAT) increased significantly (*P < 0.05). B: Relative expression of uncoupling protein 1 (*UCP1*) mRNA (**P < 0.01) (B) and β3-adrenergic receptor (*ADRB3*) mRNA (**P < 0.01) (C) in the rBAT upon Ucn1 neuron ablation, by quantitative RT-PCR.

directly affect lipolysis.

These results show that EWcp/Ucn1 neuronal ablation increases right WAT weight and the number of large adipocytes and the mean adipocyte surface area in both left and right WAT but does not directly affect lipolysis.

3.6. The effector – the impact of EWcp/LepRb/Ucn1 neurons on brown adipose tissue

As a previous study by Zhang et al. (2011) showed a direct innervation of EWcp neurons of BAT, the effect of neuron ablation on the BAT was also studied. Rats with EWcp/LepRb/Ucn1 neuron ablation had a higher right BAT weight (+57%; t(11) = -2.47; P < 0.05; control: 0.055 ± 0.009; ablation: 0.087 ± 0.009) than controls (Fig. 8A). Next, we measured UCP1-expression as a molecular marker of BAT activation and ADRB3 expression that suggests BAT-related thermogenesis via the sympathetic nervous system (Bartness and Song, 2007), using qPCR. In the right BAT, rats with EWcp/LepRb/Ucn1 neuron ablation showed a 9-times higher amount of both UCP1 mRNA (t(10) = 2.819; P < 0.01; Fig. 8B) and 16-fold elevation of ADRB3 mRNA (t(8) = 3.954; P < 0.005; Fig. 8C) than controls. No significant effect was observed for the left BAT.

These results confirm previous observations and show that EWcp/LepRb/Ucn1 neuron ablation influences BAT weight and increases UCP1 as well as ADRB3 mRNA expression in the BAT.

3.7. The effector-the impact of EWcp/LepRb/Ucn1 neurons on plasma leptin and lipid profile

In rats with EWcp/LepRb/Ucn1 ablation, the leptin plasma level tended to be higher than the controls (+51%; t(8) = −1.17; P = 0.1; control: 2.97 ± 0.8, ablation: 4.46 ± 1; n = 6; Fig. 9A). On the other

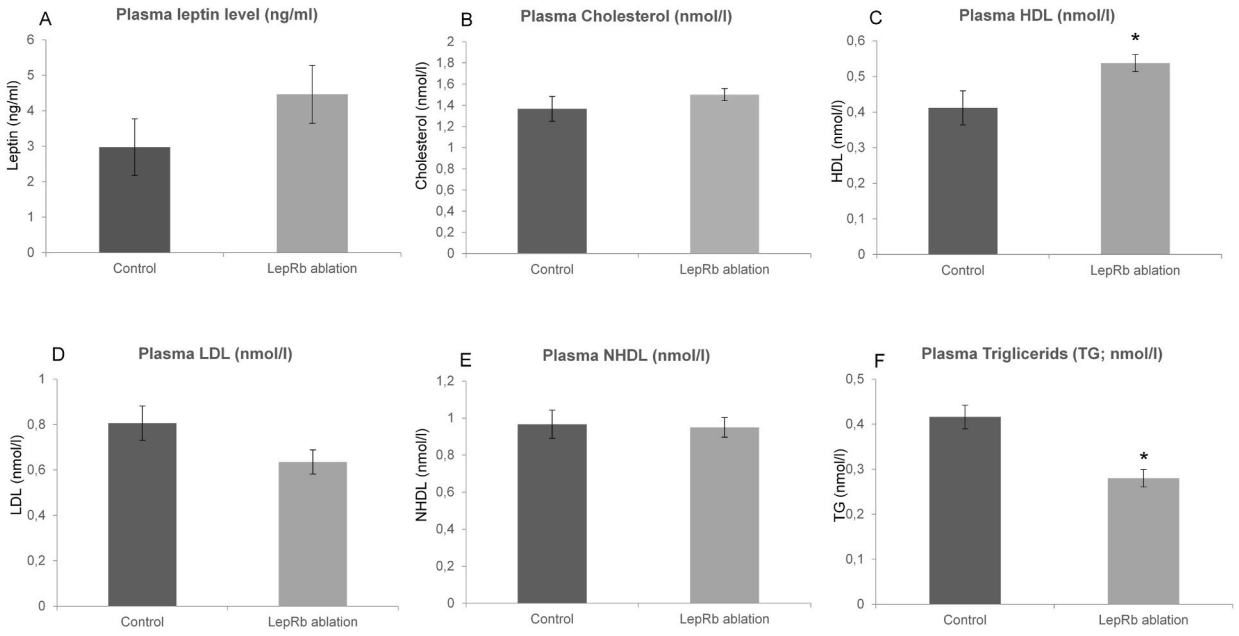

Fig. 9. Effects of EWcp/LepRb/Ucn1 neuron ablation on blood lipid profiles. Plasma leptin (A), cholesterol (B), high density lipoprotein (HDL) (C), low density lipoprotein (LDL), non-high density lipoprotein (NHDL) (D), and triglyceride (E) levels. The plasma HDL level increased (*P < 0.05) while triglyceride (*P < 0.01) deceased upon EWcp/LepRb/Ucn1 cell ablation.

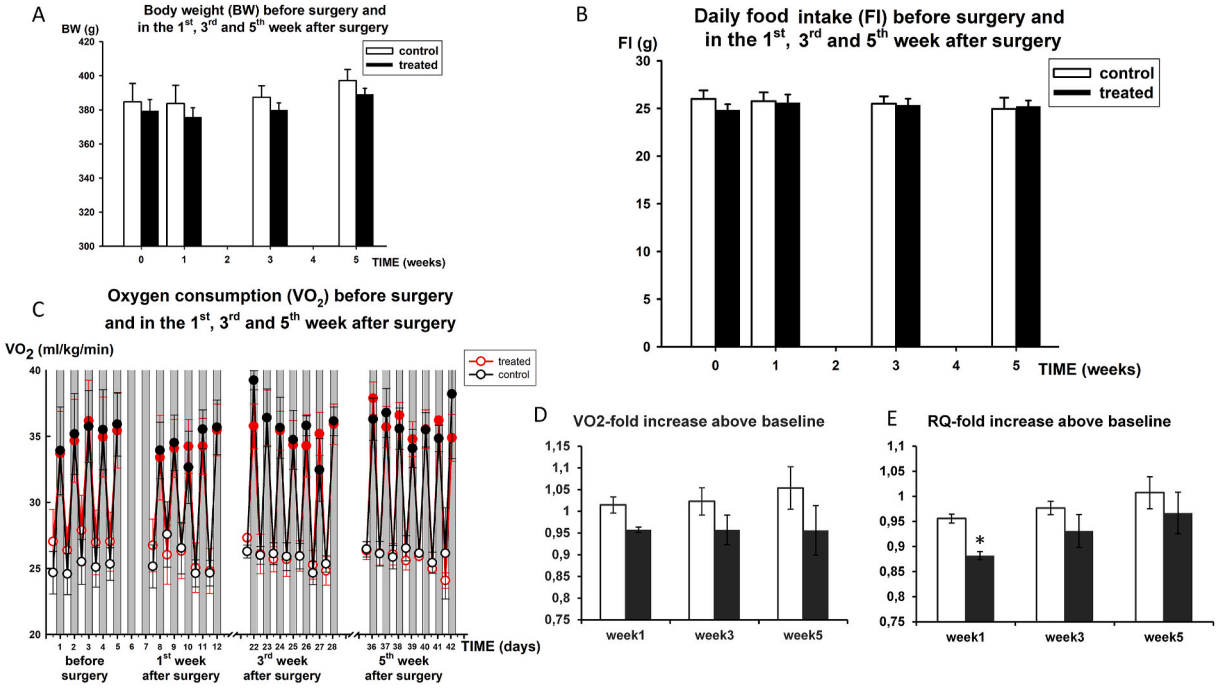

Fig. 10. Effects of EWcp/LepRb/Ucn1 neuron ablation on feeding and energy homeostasis. Bodyweight (BW) (A), food intake (B), oxygen consumption (VO_2) (C), the diurnal pattern of (VO_2) (D) and that of the respiratory quotient (RQ) (E) were assessed in saporin-injected (control) and leptin-saporin-ablated (treated) rats. One week after Ucn1 neuron ablation the RQ was significantly (*P < 0.005) reduced.

hand, circulating levels of triglycerides were clearly lower (−50%; t(10) = 3.85 P < 0.01; control: 0.42 ± 0.03; ablation: 0.28 ± 0.02; Fig. 9F). The HDL level was higher than in controls (+32%; t(10) = -2.44; P < 0.05; control: 0.41 ± 0.05; ablation: 0.54 ± 0.03; Fig. 9C), whereas the LDL level showed a strong trend towards being lower (−27%; t(9) = 2.12; P = 0.06; control: 0.81 ± 0.07; ablation: 0.64 ± 0.06; Fig. 9D). Circulating cholesterol and NHDL did not appear to have been affected by ablation (Fig. 9B, E).

These results reveal that with EWcp/LepRb/Ucn1 ablation alters plasma lipid profiles.

3.8. The effector – impact of EWcp/LepRb/Ucn1 neurons on feeding and energy homeostasis

Bodyweight and food intake parameters (see Fig. 10A) were studied during 5 weeks after leptin-saporin injection. None of these parameters

showed any significant effect of EWcp/LepRb/Ucn1 neuron ablation. Calorimetry, however, revealed a clear diurnal pattern in both ablation and control rats, as to RQ (VCO_2/VO_2) and O_2 consumption (VO_2). Both parameters were highest during the dark period (RQ; $P < 0.05$, VO2; $P < 0.001$; Fig. 10C). Furthermore, during the light period small effects of LepRb/Ucn1 neuron ablation on VO_2 (−6%; $t(5) = 1.8$; $P = 0.06$) and RQ (−8.4%; $t(5) = 5.37$; $P < 0.005$) were observed. These effects were only present during the first week after injection (Fig. 10D and E). No effects of ablation were observed at later time points.

These results demonstrate that EWcp Ucn1 neuron loss reduces respiratory quotient and oxygen consumption during the dark period.

4. Discussion

We provide evidence for a midbrain-WAT regulatory circuit via midbrain LepRb/Ucn1 neurons, supported by the following findings: 1) leptin can bind to neurons in the EWcp, 2) peripheral administration of leptin recruits pSTAT3 signaling at 2 h, and decreases pERK signaling at 4 h, 3) peripheral leptin differentially modulates the expression of Ucn1, 4) EWcp-Ucn1 neurons provide pre-sympathetic innervation to the WAT and 5) LepRb-Ucn1 neurons in the EWcp can regulate WAT and BAT structure and function in a different manner. Below these findings will be discussed in detail.

4.1. Leptin recruits different signaling pathways in EWcp neurons

We found that leptin indeed binds to its receptor in the EWcp-Ucn1 neurons, suggesting that leptin can directly regulate Ucn1 neurons' activity in the EWcp. This is corroborated by the finding that leptin treatment induced pSTAT3 at 2 h after leptin administration. However, we saw no pSTAT3 at 4 h after the injection. This activation pattern of pSTAT3 in the EWcp is in line with the temporal dynamics of leptin action in the dorsomedial and ventromedial hypothalamus (DMH, VMH; Faouzi et al., 2007), but it is in contrast to leptin-induced STAT3 phosphorylation in the ARC, which peaks already at 30 min after leptin injection and persists for at least 6 h (Guo et al., 2004). The relatively transient action of leptin on the EWcp is in line with our observation of an immediate, short-term effect of leptin on the electrical activity of the EWcp (Xu et al., 2011).

Leptin activates other signaling molecules downstream of LepRb, such as those constituting the PI3K-AKT (Niswender et al. 2001, 2004) and MAPK-ERK pathways (Rahmouni et al., 2009). In the present study, no phosphorylation of AKT was detected in the EWcp, suggesting that this pathway is not recruited by leptin action in the EWcp. This idea should not be surprising, because no changes in pAKT were observed upon leptin infusion in the hypothalamus either (Burgos-Ramos et al., 2010) and the effect of leptin on food intake, does not seem to involve AKT activation (Carvalheira et al., 2005). Concerning pERK, the picture is different. We found that 4 h after leptin injection, the amount of pERK-ir was markedly reduced compared to rats injected with saline. This effect differs from the effect of leptin on pERK in other parts of the brain. For instance, leptin rapidly (within 30 min) activates pERK in the hypothalamus, but no leptin effects are seen in extrahypothalamic nuclei like the nucleus of the solitary tract (Benomar et al., 2005; Rahmouni et al., 2009).

Nonetheless, leptin's ability to activate STAT3 indicates that it may be involved in controlling long-term transcriptional changes, such as Ucn1 gene expression. Indeed, we show that Ucn1 gene expression is induced in a time-dependent fashion by peripheral leptin. Specifically, as early as 2 h after leptin injection, Ucn1 mRNA content was elevated, and this elevation continued through 4 h after leptin injection. An increased abundance of Ucn1-ir was only observed 4 h after leptin injection. We conclude that leptin directly binds to LepRb on the EWcp/Ucn1 neurons, and induces STAT3 activation, which in turn increases Ucn1 biosynthesis evidenced by an initial increase in Ucn1 mRNA expression followed by an increase in Ucn1 peptide abundance.

Here a possible limitation of these results must be noted. The potentially painful i.p. injection may have caused some acute stress that could have affected Ucn1 mRNA and peptide abundance in EWcp cells. However, in our earlier studies we did not detect remarkable Ucn1 neuron activation upon intraperitoneal saline injection (Gaszner et al., 2004) and the acute pain-induced Ucn1 neuron activation results in a faster upregulation of Ucn1 (Rouwette et al., 2012) than observed here. Furthermore, there was a non-significant increase of Ucn1 mRNA expression 1 h after PBS injection that then gradually decreased to baseline level.

4.2. EWcp/LepRb/Ucn1 neurons regulate WAT via the autonomic nervous system

Earlier studies showed that when PRV was injected into WAT specifically, neurons in the paraventricular nucleus (PVN) and medial preoptic area (MPA) within the hypothalamus, and many nuclei in the brainstem and the spinal cord were strongly labeled (Bamshad et al., 1998). Sympathetic nerve fibers arise from the intermediolateral (IML) column of the thoracic spinal cord and project to stellate ganglia located just outside of the spinal cord. In turn, stellate ganglia give rise to postsynaptic sympathetic nerve fibers, which subsequently innervate the WAT (Geerling et al., 2014). Here we provide evidence that EWcp Ucn1 neurons were retrogradely labeled after PRV-GFP injection into WAT as well. BDG has special features compared to earlier PRV derivatives, as it shows highly specific retrograde, transneuronal spread and expresses GFP with immediate-early kinetics under the regulation of the human CMV promoter, allowing early identification of infected neurons in different brain areas. These properties are due to specific modifications of the viral genome, which have been described in detail earlier (Boldogköi et al. 2002, 2004). The route of virus infection is closely identical in the case of different target organs until the infection reaches the brain, which has been comprehensively characterized in previous studies. Thus, we have only enclosed pictures of the EWcp nucleus and have not investigated ganglia outside the spinal cord and neurons in the IML in the present paper. Viral labelling in the EWcp indicates specific and indirect neuronal control of the WAT by the EWcp. With this approach it is not possible to tell whether the connections between the EWcp and the IML are direct or indirect and this is a true limitation of the study, because they may take place partially via other autonomic nuclei in the medulla.

Another limitation we have to state is that we do not provide direct experimental evidence if the leptin-sensing EWcp/LepRb/Ucn1 are the same cells that EWcp/Ucn1 neurons project to the IML, although we assume, this is the case. Related to this, one may also argue that besides the EWcp other major Ucn1-containing brain areas (*e.g.* supraoptic nucleus, lateral superior olive; see in ref. Bittencourt et al., 1999) areas may also project to the IML. However, we could not find any published evidence that direct nerve fiber connections would exist between the supraoptic nucleus, the lateral superior olive and the IML (Tucker and Saper, 1985). Nevertheless, together with the fact that Ucn1 fibers innervate the sympathetic outflow area of the thoracic spinal cord (Korosi et al., 2007), support the view that EWcp is one of the brain regions that regulate SNS components (Cano et al., 2021).

In general, increased sympathetic output from the SNS toward WAT increases plasma TG levels by stimulating hepatic VLDL production, and lipolysis in WAT. The latter results in the release of free fatty acids (FFA), which are transported to the liver to fuel the increased synthesis of VLDL. Ablation of LepRb/Ucn1 neurons resulted in significant WAT weight increase due to an increase in adipocyte size. Also, compared to control rats, rats with EWcp/LepRb/Ucn1 neuron ablation had lower plasma TG, lower LDL and HDL, which is probably due to decreased lipolytic activity. Decreased lipolysis leads to a decrease in circulating FFA, which results in a substrate shortage for hepatic very-low-density lipoprotein (VLDL) production, consequently reducing plasma levels of LDL and TG and increased plasma HDL. Taken together, the fat mass and

plasma lipid analysis suggest that the ablation of LepRb/Ucn1 neurons in the EWcp leads to an overall decrease in lipolysis, indicating a decrease in the SNS outflow to WAT.

To gain more insights into the regulation of EWcp on adipose metabolism, we further investigated the BAT in the rats with EWcp/LepRb/Ucn1 ablation. The SNS densely innervates the BAT, and SNS-mediated BAT thermogenesis is controlled by various brain areas (Boulant, 2000; Watanabe et al., 1994). Norepinephrine (NE) from SNS terminals stimulates ADRB3-activated BAT thermogenesis (Bartness and Song, 2007), enhances expression and synthesis of uncoupling protein-1 (UCP1). We found that the ablation of LepRb/Ucn1 neurons resulted in significant BAT weight increase. In addition, rats with EWcp/LepRb/Ucn1 neuron ablation showed an increased expression of ADRB3 mRNA and UCP1 mRNA in the BAT, suggesting BAT activation happens indeed through an increased SNS activity. These findings corroborate that the EWcp/LepRB/Ucn1 cells contribute to the higher-order control of SNS and BAT thermogenesis that is in agreement with our recent finding that local injection of melanocortin 4 receptor agonists activates EWcp/Ucn1 neurons, leading to the rise of energy metabolism and heat loss via increased peripheral vasodilation (Füredi et al., 2017).

When compiling collected data from WAT and BAT, a paradoxical picture emerges at first sight. On one hand, the EWcp seems to be a brain site involved in adipose metabolism regulation through controlling SNS activity. On the other hand, data of ADRB3 and UCP1 induction would suggest increased SNS innervations to the BAT. Although these data may seem paradoxical, when we consider that animals were all sacrificed two weeks after the surgery, we could propose a potential mechanism to resolve this paradox. Specifically, we suggest that the ablation of EWcp/LepRb/Ucn1 neurons leads to a decreased Ucn1 output towards the SNS. Decreased SNS activity in WAT leads to decreased TG levels and decreased lipolysis resulting in increased WAT size. The concomitant increase in leptin, however, is unable to upregulate Ucn1 production because of the ablation of EWcp/LepRb/Ucn1 neurons. However, leptin would still be able to reach other hypothalamic nuclei to activate the BAT. These results indicate that BAT activation is not primarily regulated by the EWcp/LepRb/Ucn1 neurons, but by the effect of leptin outside the EWcp.

4.3. Involvement of EWcp/LepRb/Ucn1 EWcp in energy balance

Maintenance of energy homeostasis and body weight is achieved by an intricate balance between energy intake (food intake) and expenditure. The ablation of LepRb/Ucn1 neurons in the EWcp has no apparent impact on food intake and body weight. Although not significant, these observations suggest an important notion that the effect of EWcp/LepRb/Ucn1 ablation is independent of leptin/Ucn1 anorexic effects. Earlier studies have found that central administration of Ucn1 results in a potent suppression of food intake (Spina et al., 1996) and increases whole-body oxygen consumption (De Fanti and Martínez, 2002). Interestingly, the fact that within the first week after the surgery, reduced LepRb/Ucn1 expression in the EWcp has led to a transient decrease in respiratory quotient (RQ, indicative of increased fat usage) in the light period; effects that were not seen for the remaining of the experiment, suggests that EWcp/LepRb/Ucn1 neurons modulate specifically WAT lipid mobilization and fat oxidation. In addition to this role of EWcp/LepRb/Ucn1 neurons, recently we have shown that they also contribute to energy intake/expenditure (Füredi et al., 2017).

4.4. Conclusions and future perspectives

Internal states, such as *e.g.* fight-or-flight response, profoundly influence physiology and behavior. A study by Lovett-Barron et al. (2017) identified a set of diverse neuromodulatory systems, including the EWcp governing internal states. The data summarized in this study indicate that WAT-derived leptin binds to the LepRb in the EWcp, increases Ucn1 production in the EWcp, and leads to enhanced sympathetic innervation of WAT. This leads to increased plasma TG levels as well as lipolysis in WAT without altering food intake. Collectively, we propose that the EWcp mediated activation of SNS is required to maintain energy homeostasis under different internal states (*e.g.* fight-or-flight response; Kozicz et al., 2011 and Xu, 2014) in which an organism needs to recruit fuels without being able to eat.

Author contributions

LX and B Geenen performed the histological techniques, PCR experiments, evaluated the results and performed the statistics. LX wrote the manuscript draft. NF, CL performed the animal surgery, metabolic measurements and immunocytochemistry. EP and MB supervised the metabolic experiments, evaluated the results and prepared the corresponding figures. ÁD performed the virus injections and evaluated the related results. KJK supervised virus injections and approved the draft manuscript. BG performed and supervised the animal experiments, collected tissue samples, performed the histological techniques and morphometry. TK designed the experiments, supervised data assessment, edited the final version of manuscript which was approved by all authors.

Acknowledgements

NF was supported by the research grant of Pecs University Medical School KA-2020-03, and New National Excellence Program of the Ministry for Innovation and Technology from the source of the National Research, Development and Innovation Fund (ÚNKP-20-4-II-PTE-547). EP was supported by the grant from the Pécs University Medical School KA-2019-44. KJK was supported by Hungarian National Research, Development and Innovation Office (124424), and National Brain Research Program 2017-1.2.1-NKP-2017-00002. BG was financed by the Project no. TKP2020-IKA-08 provided from the National Research, Development and Innovation Fund of Hungary, financed under the 2020-4.1.1-TKP2020 funding scheme. (FIKP II, FIKP III), EFOP-3.6.2-16-2017-00008 and NKFIH FK124188. This work was also financed by NAP 2017-1.2.1-NKP-2017-00002; GINOP-2.3.2-15-2016-00050 "PEPSYS," and MTA-TKI14016.

Appendix A. Supplementary data

Supplementary data to this article can be found online at https://doi.org/10.1016/j.neuropharm.2021.108898.

References

Bamshad, M., Aoki, V.T., Adkison, M.G., Warren, W.S., Bartness, T.J., 1998. Central nervous system origins of the sympathetic nervous system outflow to white adipose tissue. Am. J. Physiol. 275 (1 Pt 2), R291–R299.

Banks, W.A., Clever, C.M., Farrell, C.L., 2000. Partial saturation and regional variation in the blood-to-brain transport of leptin in normal weight mice. Am. J. Physiol. Endocrinol. Metab. 278 (6), E1158–E1165.

Bartness, T.J., Song, C.K., 2007. Brain-adipose tissue neural crosstalk. Physiol. Behav. 91 (4), 343–351.

Benoit, S.C., Thiele, T.E., Heinrichs, S.C., Rushing, P.A., Blake, K.A., Steeley, R.J., 2000. Comparison of central administration of corticotropin-releasing hormone and urocortin on food intake, conditioned taste aversion, and c-Fos expression. Peptides 21 (3), 345–351.

Benomar, Y., Wetzler, S., Larue-Achagiotis, C., Djiane, J., Tomé, D., Taouis, M., 2005. In vivo leptin infusion impairs insulin and leptin signalling in liver and hypothalamus. Mol. Cell. Endocrinol. 242 (1–2), 59–66.

Bittencourt, J.C., Vaughan, J., Arias, C., Rissman, R.A., Vale, W.W., Sawchenko, P.E., 1999. Urocortin expression in rat brain: evidence against a pervasive relationship of urocortin-containing projections with targets bearing type 2 CRF receptors. J. Comp. Neurol. 415 (3), 285–312.

Boldogköi, Z., Reichart, A., Tóth, I.E., Sik, A., Erdélyi, F., Medveczky, I., Llorens-Cortes, C., Palkovits, M., Lenkei, Z., 2002. Construction of recombinant pseudorabies viruses optimized for labeling and neurochemical characterization of neural circuitry. Brain Res Mol Brain Res 109 (1–2), 105–118.

Boldogköi, Z., Sík, A., Dénes, A., Reichart, A., Toldi, J., Gerendai, I., Kovács, K.J., Palkovits, M., 2004. Novel tracing paradigms–genetically engineered herpesviruses

as tools for mapping functional circuits within the CNS: present status and future prospects. Prog. Neurobiol. 72 (6), 417–445.
Boulant, J.A., 2000. Role of the preoptic-anterior hypothalamus in thermoregulation and fever. Clin. Infect. Dis. 31 (Suppl. 5), S157–S161.
Burgos-Ramos, E., Chowen, J.A., Argente, J., Barrios, V., 2010. Regional and temporal differences in leptin signaling in rat brain. Gen. Comp. Endocrinol. 167 (1), 143–152.
Cano, G., Sved, A.F., Rinaman, L., Rabin, B.S., Card, J.P., 2001. Characterization of the central nervous system innervation of the rat spleen using viral transneuronal tracing. J. Comp. Neurol. 439 (1), 1–18.
Cano, G., Hernan, S.L., Sved, A.F., 2021. Centrally projecting Edinger-Westphal nucleus in the control of sympathetic outflow and energy homeostasis. Brain Sci. 11 (8), 1005.
Caron, E., Sachot, C., Prevot, V., Bouret, S.G., 2010. Distribution of leptin-sensitive cells in the postnatal and adult mouse brain. J. Comp. Neurol. 518 (4), 459–476.
Carvalheira, J.B., Torsoni, M.A., Ueno, M., Amaral, M.E., Araújo, E.P., Velloso, L.A., Gontijo, J.A., Saad, M.J., 2005. Cross-talk between the insulin and leptin signaling systems in rat hypothalamus. Obes. Res. 13 (1), 48–57.
De Fanti, B.A., Martínez, J.A., 2002. Central urocortin activation of sympathetic-regulated energy metabolism in Wistar rats. Brain Res. 930 (1–2), 37–41.
Dénes, A., Boldogkoi, Z., Uhereczky, G., Hornyák, A., Rusvai, M., Palkovits, M., Kovács, K.J., 2005. Central autonomic control of the bone marrow: multisynaptic tract tracing by recombinant pseudorabies virus. Neuroscience 134 (3), 947–963.
Dénes, A., Boldogkoi, Z., Hornyák, A., Palkovits, M., Kovács, K.J., 2006 Nov. Attenuated pseudorabies virus-evoked rapid innate immune response in the rat brain. J. Neuroimmunol. 180 (1–2), 88–103.
Derks, N.M., Müller, M., Gaszner, B., Tilburg-Ouwens, D.T., Roubos, E.W., Kozicz, L.T., 2008. Housekeeping genes revisited: different expressions depending on gender, brain area and stressor. Neuroscience 156, 305–309.
Derks, N.M., Gaszner, B., Roubos, E.W., Kozicz, L.T., 2010. Sex differences in urocortin 1 dynamics in the non-preganglionic Edinger-Westphal nucleus of the rat. Neurosci. Res. 66 (1), 117–123.
Elmquist, J.K., Bjørbaek, C., Ahima, R.S., Flier, J.S., Saper, C.B., 1998. Distributions of leptin receptor mRNA isoforms in the rat brain. J. Comp. Neurol. 395 (4), 535–547.
Faouzi, M., Leshan, R., Björnholm, M., Hennessey, T., Jones, J., Münzberg, H., 2007. Differential accessibility of circulating leptin to individual hypothalamic sites. Endocrinology 148 (11), 5414–5423.
Farkas, E., Jansen, A.S., Loewy, A.D., 1998. Periaqueductal gray matter input to cardiac-related sympathetic premotor neurons. Brain Res. 792 (2), 179–192.
Figlewicz, D.P., Bennett, J.L., Naleid, A.M., Davis, C., Grimm, J.W., 2006. Intraventricular insulin and leptin decrease sucrose self-administration in rats. Physiol. Behav. 89 (4), 611–616.
Füredi, N., Nagy, Á., Mikó, A., Berta, G., Kozicz, T., Pétervári, E., Balaskó, M., Gaszner, B., 2017 May 15. Melanocortin 4 receptor ligands modulate energy homeostasis through urocortin 1 neurons of the centrally projecting Edinger-Westphal nucleus. Neuropharmacology 118, 26–37.
Gao, Q., Horvath, T.L., 2007. Neurobiology of feeding and energy expenditure. Annu. Rev. Neurosci. 30, 367–398.
Gaszner, B., Csernus, V., Kozicz, T., 2004. Urocortinergic neurons respond in a differentiated manner to various acute stressors in the Edinger–Westphal nucleus in the rat. J. Comp. Neurol. 480 (2), 170–179.
Geerling, J.J., Boon, M.R., Kooijman, S., Parlevliet, E.T., Havekes, L.M., Romijn, J.A., Meurs, I.M., Rensen, P.C., 2014. Sympathetic nervous system control of triglyceride metabolism: novel concepts derived from recent studies. J. Lipid Res. 55 (2), 180–189.
Guo, F., Bakal, K., Minokoshi, Y., Hollenberg, A.N., 2004. Leptin signaling targets the thyrotropin-releasing hormone gene promoter in vivo. Endocrinology 145 (5), 2221–2227.
Jansen, A.S., Hoffman, J.L., Loewy, A.D., 1997. CNS sites involved in sympathetic and parasympathetic control of the pancreas: a viral tracing study. Brain Res. 766 (1–2), 29–38.
Kieffer, T.J., Heller, R.S., Leech, C.A., Holz, G.G., Habener, J.F., 1997 Jun. Leptin suppression of insulin secretion by the activation of ATP-sensitive K+ channels in pancreatic beta-cells. Diabetes 46 (6), 1087–1093.
Klooster, J., Beckers, H.J., Vrensen, G.F., van der Want, J.J., 1993. The peripheral and central projections of the Edinger–Westphal nucleus in the rat. A light and electron microscopic tracing study. Brain Res. 632 (1–2), 260–273.
Korosi, A., Schotanus, S., Olivier, B., Roubos, E.W., Kozicz, T., 2005. Chronic ether stress-induced response of urocortin1 neurons in the Edinger–Westphal nucleus in the mouse. Brain Res. 1046, 172–179.
Korosi, A., Kozicz, T., Richter, J., Veening, J.G., Olivier, B., Roubos, E.W., 2007. Corticotropin-releasing factor, urocortin 1, and their receptors in the mouse spinal cord. J. Comp. Neurol. 502 (6), 973–989.
Kozicz, T., 2007. On the role of urocortin 1 in the non-preganglionic Edinger–Westphal nucleus in stress adaptation. Gen. Comp. Endocrinol. 153 (1–3), 235–240.
Kozicz, T., Yanaihara, H., Arimura, A., 1998. Distribution of urocortin-like immunoreactivity in the central nervous system of the rat. J. Comp. Neurol. 391 (1), 1–10.
Kozicz, T., Li, M., Arimura, A., 2001. The activation of urocortin immunoreactive neurons in the Edinger–Westphal nucleus following stress in rats. Stress 4 (2), 85–90.
Kozicz, T., Bittencourt, J.C., May, P.J., Reiner, A., Gamlin, P.D., Palkovits, M., Horn, A. K., Toledo, C.A., Ryabinin, A.E., 2011a. The Edinger-Westphal nucleus: a historical, structural, and functional perspective on a dichotomous terminology. J. Comp. Neurol. 519 (8), 1413–1434.
Kozicz, T., Sterrenburg, L., Xu, L., 2011b. Does midbrain urocortin 1 matter? A 15-year journey from stress (mal)adaptation to energy metabolism. Stress 14 (4), 376–383.
Kuperman, Y., Chen, A., 2008. Urocortins: emerging metabolic and energy homeostasis perspectives. Trends Endocrinol. Metabol. 19 (4), 122–129.
Leinninger, G.M., Jo, Y.H., Leshan, R.L., Louis, G.W., Yang, H., Barrera, J.G., Wilson, H., Opland, D.M., Faouzi, M.A., Gong, Y., Jones, J.C., Rhodes, C.J., Chua Jr., S., Diano, S., Horvath, T.L., Seeley, R.J., Becker, J.B., Münzberg, H., Myers Jr., M.G., 2009. Leptin acts via leptin receptor-expressing lateral hypothalamic neurons to modulate the mesolimbic dopamine system and suppress feeding. Cell Metabol. 10 (2), 89–98.
Liu, J., Yang, X., Yu, S., Zheng, R., 2018. The leptin signaling. Adv. Exp. Med. Biol. 1090, 123–144.
Lovett-Barron, M., Andalman, A.S., Allen, W.E., Vesuna, S., Kauvar, I., Burns, V.M., Deisseroth, K., 2017 Nov 30. Ancestral circuits for the coordinated modulation of brain state. Cell 171 (6), 1411–1423 e17.
Morton, G.J., Cummings, D.E., Baskin, D.G., Barsh, G.S., Schwartz, M.W., 2006. Central nervous system control of food intake and body weight. Nature 443 (7109), 289–295.
Myers Jr., M.G., Münzberg, H., Leinninger, G.M., Leshan, R.L., 2009. The geometry of leptin action in the brain: more complicated than a simple ARC. Cell Metabol. 9 (2), 117–123.
Niswender, K.D., Morton, G.J., Stearns, W.H., Rhodes, C.J., Myers Jr., M.G., Schwartz, M. W., 2001. Intracellular signalling. Key enzyme in leptin-induced anorexia. Nature 413 (6858), 794–795.
Niswender, K.D., Baskin, D.G., Schwartz, M.W., 2004. Insulin and its evolving partnership with leptin in the hypothalamic control of energy homeostasis. Trends Endocrinol. Metabol. 15 (8), 362–369.
Paxinos, G., Franklin, K., 2003. The Mouse Brain in Stereotaxic Coordinatres, third ed. Elsevier Academic, San Diego, ISBN 0123694604.
Rahmouni, K., Sigmund, C.D., Haynes, W.G., Mark, A.L., 2009. Hypothalamic ERK mediates the anorectic and thermogenic sympathetic effects of leptin. Diabetes 58 (3), 536–542.
Rizk, N.M., Stammsen, D., Preibisch, G., Eckel, J., 2001. Leptin and tumor necrosis factor-α induce the tyrosine phosphorylation of signal transducer and activator of transcription proteins in the hypothalamus of normal rats in vivo. Endocrinology 142, 3027–3032.
Rouwette, T., Klemann, K., Gaszner, B., Scheffer, G.J., Roubos, E.W., Scheenen, W.J., et al., 2011. Differential responses of corticotropin-releasing factor and urocortin 1 to acute pain stress in the rat brain. Neuroscience 183, 15–24.
Rouwette, T., Vanelderen, P., de Reus, M., Loohuis, N.O., Giele, J., van Egmond, J., Scheenen, W., Scheffer, G.J., Roubos, E., Vissers, K., Kozicz, T., 2012. Experimental neuropathy increases limbic forebrain CRF. Eur. J. Pain 16 (1), 61–71.
Ryabinin, A.E., Weitemier, A.Z., 2006. The urocortin 1 neurocircuit: ethanol-sensitivity and potential involvement in alcohol consumption. Brain Res. Rev. 52 (2), 368–380.
Scott, M.M., Lachey, J.L., Sternson, S.M., Lee, C.E., Elias, C.F., Friedman, J.M., Elmquist, J.K., 2009. Leptin targets in the mouse brain. J. Comp. Neurol. 514 (5), 518–532.
Shah, N.S., Pugh, P.C., Nam, H., Rosenthal, D.T., van Wijk, D., Gaszner, B., Kozicz, T., Kerman, I.A., 2013. A subset of presympathetic-premotor neurons within the centrally projecting Edinger-Westphal nucleus expresses urocortin-1. J. Chem. Neuroanat. 52, 25–35.
Shapiro, S.S., Wilk, M.B., 1965. An analysis of variance test for normality. Biometrika 52, 591–599.
Simerly, R.B., 2008. Hypothalamic substrates of metabolic imprinting. Physiol. Behav. 94 (1), 79–89.
Snedecor, G.W., Cochran, W.G., 1989. Statistical Methods. Iowa State University Press.
Spina, M., Merlo-Pich, E., Chan, R.K., Basso, A.M., Rivier, J., Vale, W., Koob, G.F., 1996. Appetite-suppressing effects of urocortin, a CRF-related neuropeptide. Science 273 (5281), 1561–1564.
Tucker, D.C., Saper, C.B., 1985. Specificity of spinal projections from hypothalamic and brainstem areas which innervate sympathetic preganglionic neurons. Brain Res. 360 (1–2), 159–164.
Turek, V.F., Ryabinin, A.E., 2005. Expression of c-Fos in the mouse Edinger-Westphal nucleus following ethanol administration is not secondary to hypothermia or stress. Brain Res. 1063 (2), 132–139.
Villanueva, E.C., Myers Jr., M.G., 2008. Leptin receptor signaling and the regulation of mammalian physiology. Int. J. Obes. (Lond.) 32 (Suppl 7), S8–12.
Wang, C., Mullet, M.A., Glass, M.J., Billington, C.J., Levine, A.S., Kotz, C.M., 2001. Feeding inhibition by urocortin in the rat hypothalamic paraventricular nucleus. Am. J. Physiol. Regul. Integr. Comp. Physiol. 280 (2), R473–R480.
Warwick, R., 1954. The ocular parasympathetic nerve supply and its mesencephalic sources. J. Anat. 88 (1), 71–93.
Watanabe, J., Mishiro, K., Amatsu, T., Kanamura, S., 1994. Absence of paravascular nerve projection and cross-innervation in interscapular brown adipose tissues of mice. J. Auton. Nerv. Syst. 49 (3), 269–276.
Xu, L., 2014. Leptin action in the midbrain: from reward to stress. J. Chem. Neuroanat. 61–62, 256–265.
Xu, L., Bloem, B., Gaszner, B., Roubos, E.W., Kozicz, T., 2009. Sex-specific effects of fasting on urocortin 1, cocaine- and amphetamine-regulated transcript peptide and nesfatin-1 expression in the rat Edinger–Westphal nucleus. Neuroscience 162 (4), 1141–1149.
Xu, L., Bloem, B., Gaszner, B., Roubos, E.W., Kozicz, T., 2010. Stress- related changes in the activity of cocaine- and amphetamine-regulated transcript and nesfatin neurons in the midbrain non-preganglionic Edinger–Westphal nucleus in the rat. Neuroscience 170, 478–488.
Xu, L., Scheenen, W.J., Leshan, R.L., Patterson, C.M., Elias, C.F., Bouwhuis, S., Roubos, E. W., Myers Jr., M.G., Kozicz, T., 2011. Leptin signaling modulates the activity of

urocortin 1 neurons in the mouse nonpreganglionic Edinger–Westphal nucleus. Endocrinology 152 (3), 979–988.
Xu, L., Scheenen, W.J., Roubos, E.W., Kozicz, T., 2012. Peptidergic Edinger-Westphal neurons and the energy-dependent stress response. Gen. Comp. Endocrinol. 177 (3), 296–304.
Xu, L., Janssen, D., van der Knaap, N., Roubos, E.W., Leshan, R.L., Myers Jr., M.G., Gaszner, B., Kozicz, T., 2014. Integration of stress and leptin signaling by CART producing neurons in the rodent midbrain centrally projecting Edinger-Westphal nucleus. Front. Neuroanat. 8, 8. https://doi.org/10.3389/fnana.2014.00008.
Zeng, W., Pirzgalska, R.M., Pereira, M.M., Kubasova, N., Barateiro, A., Seixas, E., Lu, Y. H., Kozlova, A., Voss, H., Martins, G.G., Friedman, J.M., Domingos, A.I., 2015. Sympathetic neuro-adipose connections mediate leptin-driven lipolysis. Cell 163 (1), 84–94.
Zhang, Y., Proenca, R., Maffei, M., Barone, M., Leopold, L., Friedman, J.M., 1994. Positional cloning of the mouse obese gene and its human homologue. Nature 372 (6505), 425–432.
Zhang, Y., Kerman, I.A., Laque, A., Nguyen, P., Faouzi, M., Louis, G.W., Jones, J.C., Rhodes, C., Münzberg, H., 2011 Feb 2. Leptin-receptor-expressing neurons in the dorsomedial hypothalamus and median preoptic area regulate sympathetic brown adipose tissue circuits. J. Neurosci. 31 (5), 1873–1884. https://doi.org/10.1523/JNEUROSCI.3223-10.2011. PMID: 21289197; PMCID: PMC3069639.
Zhang, W., Cline, M.A., Gilbert, E.R., 2014. Hypothalamus-adipose tissue crosstalk: neuropeptide Y and the regulation of energy metabolism. Nutr. Metab. 11, 27. https://doi.org/10.1186/1743-7075-11-27.